Available online at www.sciencedirect.com

ScienceDirect

Advances in Space Research xxx (xxxx) xxx

ADVANCES IN SPACE RESEARCH (a COSPAR publication)

www.elsevier.com/locate/asr

Extended Kalman filters for close-range navigation to noncooperative targets

Gabriella Gaias *, Marco Lovera

Department of Aerospace Science and Technology, Politecnico di Milano, Via La Masa 34, 20156 Milano, Italy

Received 11 November 2022; received in revised form 16 October 2023; accepted 23 October 2023

Abstract

This work presents a set of dynamic filters for estimating the relative roto-translational state and the main parameters of a noncooperative target from an observing chaser satellite during close proximity operations. The proposed different options address a wide range of design possibilities for the architecture of the relative navigation system. All filters are derived from a common, general, core shaped as a dynamic multiplicative extended Kalman filter using dual quaternions. This allows exploiting the advantages of handling the pose (*i.e.*, attitude and position) in a multiplicative fashion, while improving the accuracy in the estimation of the angular and linear relative velocities, as well as enabling the estimation of some meaningful parameters of the target spacecraft (*e.g.*, the ratios of the moments of inertia, position and orientation of the principal axes frame). Moreover, by adopting relative kinematics and dynamics equations in dual quaternions, the inherent coupling of the six degrees-of-freedom motion is addressed with no approximations. All filters take as observations only the noisy pose measurements from an electro-optical device. For each proposed formulation, numerical simulations are carried out to show the behavior of the filter within a scenario representative of close-range target inspection at conclusion of the mid-range rendezvous.

Keywords: Active debris removal; Relative state estimation; Parameters estimation; Extended Kalman filter; Dual quaternions

1. Introduction

Several multi-satellite missions that require close proximity operations (CPOs) are currently under consideration by the space community. These span from on-orbit servicing activities to inspect, repair, and therefore provide life extension to damaged satellites to active debris removal missions devoted to guarantee the long-term sustainability of the space environment (*e.g.*, removal of critical large inoperative targets, periodical support to large constellation assets). The time and space scales of CPOs demand for the capability to estimate onboard and in real-time the relative 6 degree-of-freedom (DoF) relative state between the target and chaser satellites. In addition, some critical phases such as final approach and capture of the target rely on a motion planning based on the prediction obtained propagating in time the estimated solution. Accordingly, to guarantee the accuracy needed, mass inertia properties and location of the center of mass of the target should be also known. Since inoperative satellites are *de facto* partially unknown targets - due to possible damages, unknown status at end of life, and system deterioration in space - the estimation of the main target parameters becomes also necessary during CPOs.

The architecture of the close-range relative navigation system mainly depends on the level of cooperation of the target satellite (Opromolla et al., 2017). Disregarding the detailed design, a filtering scheme is always a key building

* Corresponding author.
E-mail addresses: gabriella.gaias@polimi.it (G. Gaias), marco.lovera@polimi.it (M. Lovera).

https://doi.org/10.1016/j.asr.2023.10.038
0273-1177/

block to refine the information provided by the sensing devices and to perform a motion prediction in case of data gaps in the observations. In this work the focus is on *non-cooperative* targets, which can be inoperative satellites or spacecraft not designed to actively support CPOs. In this case, the navigation system can only employ (active and/or passive) electro-optical sensors to observe the target object (Opromolla et al., 2017). The common feature of these devices is the impossibility to perform a direct measurement of the relative angular rate nor of the relative linear velocity w.r.t. the target. The architecture of close-range relative navigation systems can be categorized into loosely- and tightly-coupled design approaches (Opromolla et al., 2017; Pasqualetto Cassinis et al., 2019; Pasqualetto Cassinis et al., 2021). In the first option, the state/parameters estimation and the filtering scheme are addressed by two separate sequential functional blocks. Accordingly, the sensor data processing unit provides a set of pseudo-measurements to the filter, which then incorporates them in the measurement update step. In the tightly-coupled configuration, instead, the sensors' data processing and the filtering task are performed by a single functional block. Hence, the observations are the direct measures of features detected on the target. This work proposes a filtering scheme whose general structure can serve crosswise the aforementioned possible architectures of the close-range navigation system, with the possibility to refine the knowledge of the parameters while reconstructing the 6 DoF relative state.

An overview of the navigation filters for CPOs investigated in recent years to perform relative pose (*i.e.*, position and attitude) estimation is provided in Pasqualetto Cassinis et al. (2019): the general approach is to design two separate filters to estimate the translational and rotational motions. The identification of target's parameters is also mainly addressed as a separate problem. For example, Sheinfeld and Rock (2009) and Benninghoff and Boge (2015), respectively propose a free and a constrained least squares problem for the estimation of the location of the center of mass and the moments of inertia. Nonetheless, both works lack realism since they assume to know all the dynamical quantities (with noise). Overall, the implementation of different filters specialized on specific relative navigation related sub-problems impacts the complexity of the whole guidance navigation and control (GNC) system. It increases the number of sub-units, interfaces between them, GNC operative modes, and complexity of the correlations between GNC modes and phases of the CPOs (*e.g.*, inspection, final approach, capture). Specifically, this design philosophy introduces an artificial splitting of phenomena that are interconnected: the relative translational motion depends on the rotational one and the rotational dynamics is function of the inertia properties of the target body. This leads to introducing approximations that may impact the quality of the estimated solution in terms of achievable accuracy and robustness of the estimation process.

As for the simultaneous estimation of the 6 DoF state and target parameters, Aghili and Parsa (2009) proposed an additive, discrete, noise adaptive, extended Kalman filter (EKF). Such filter receives the measurements of a feature detected on the target to deliver full state, ratios of the inertia moments, and position and orientation of the target principal axes frame. The peculiarity of their approach is to structure the state so that most of the parameters appear in the observation matrix rather than in the system dynamics. Nonetheless, they introduce several approximations on the motion. The relative translational dynamics is described through the Clohessy-Wiltshire equations, which decouples the translational and rotational sub-parts of the state transition matrix. The chaser is assumed controlled to follow a constant angular rate, which makes the time derivative of the relative error quaternion function of the absolute angular rate of the target rather than of the relative one. This explains the hybrid formulation of the rotational state where the variables are the relative quaternion and the absolute angular rate of the target. Pesce et al. (2017) proposed an algorithm to estimate pose and target inertia properties, though it is specifically suited for the vision-based stereo-vision application.

As for the consideration of the inherent coupling between rotational and translational motions, several works exploited the dual quaternion (DQ) framework. The DQ, in fact, is a compact representation of the roto-translational displacement between a couple of reference systems and the DQ algebra allows handling the rotation-translation components through the same operations. In this context, Filipe et al. (2015) proposed a kinematic-only DQ-based multiplicative extended Kalman filter (MEKF). It is designed as a continuous-discrete Kalman filter, which can be specified to the case where the observations are only the relative pose between the target and chaser satellites. They showed that handling the whole pose is a multiplicative fashion, through the DQ formulation and the extension of the error quaternion concept to DQs, improves the pose estimation accuracy for small values of the measurement update rate, which is likely to occur in noncooperative CPOs. Hou et al. (2017) proposed a DQ EKF to estimate 6 DoF state, target inertia ratios, and location of the center of mass. In their formulation the absolute state of the target appears in the filter state. Accordingly, the kinematic part retains the approach of Filipe et al. (2015), since it is independent from the choice of the considered reference systems. The dynamics part is included as in Aghili and Parsa (2009), though written as the DQ-based absolute dynamics of the target. As for the measurement equations, the observations are expressed in the inertial frame. This implies that the covariance matrix of the measurements should take into account also the the errors on the knowledge of the chaser's attitude and absolute position, since the relative navigation sensors are embarked on the chaser spacecraft. In addition, as the ori-

entation of the target's principal axes frame is not estimated, there is the implicit hypothesis that the arbitrary frame w.r.t. which the observations are taken is directly the principal frame of the target. It is emphasized that, the DQ representation combines linear and angular quantities. Hence, when the absolute state of a satellite is used, the numerical values of the variables associated with linear and angular motions have rather different scales and, if not properly handled, the DQ operations would introduce on the rotational part non-negligible numerical errors. A further work exploiting the DQ formulation has been proposed by Yuan et al. (2019). This employes the approach of Hou et al. (2017), though considering two satellites observing the target object in order to implement a fault-tolerant federal EKF strategy. Clearly this requires a very specific design of the space segment, making it not applicable to the standard case of one chaser observing the target object. Razgus et al., 2017 developed a DQ EKF for the relative navigation during asteroid circumnavigation, showing capability to estimate in a more accurate fashion the relative pose and gyroscope's drifts compared to a conventional Cartesian filter development. Nonetheless, the satellite relative dynamics around the asteroid is modeled as a perturbed two-body problem (with the asteroid as the main attractor), which in this paper is denoted as to the absolute rigid body dynamics. Accordingly, such filter development cannot be applied to the satellite CPOs case. Moreover, the measurement update step in such asteroid application benefits from the availability of gyroscopes to provide a direct measurement of the angular rate. So far, the relative dynamic equations in DQ have been used to design 6 DoF controllers for target tracking and formation flying applications (Filipe and Tsiotras, 2015; Wang and Sun, 2012). As far as the authors know, there are no applications of satellite relative navigation that take advantage of the DQ-based relative dynamic equations.

This work presents a dynamic filtering scheme for simultaneous relative 6 DoF state and parameters estimation using dual quaternions. In particular, since both measurement and relative dynamics equations are nonlinear functions of the state, the EKF technique has been adopted, in view of possible future spaceborne applications. The core filter is developed in continuous time with discrete measurement models. This approach has been chosen in preparation of supporting future applications in which more sensors are used, with possibly different measurement rates. The inherent coupling between the translational and rotational motions is taken into account by employing the DQ parametrization and no approximations on the motion are introduced. Moreover, the DQ formulation renders the 6 DoF relative dynamics equations in a very compact and simple fashion, formally equivalent to the quaternion-based rotation-only relative dynamics. Indeed, the complexity in play is embedded into the dual quaternion algebra. In the paper it is shown that, by expanding the DQ-based equations in components, the relative translation dynamics simplifies to the difference of the absolute translation dynamics of the two satellites. If the Cartesian relative angular rate, position, and linear velocity were used in the state, instead, a convenient choice to obtain compact 6 DoF equations would be to derive the rotation-only part as in Segal and Gurfil (2009) and the relative translation in the moving frame attached to the target s/c. Although this result is also quite compact, the advantage of handling the rotation-translation components through the same operations is lost.

As a result, the original contributions of this work can be summarized as follows:

1. the development of a dynamic version of the DQ MEKF able to improve the accuracy of the estimation of the dual velocity component and to enable the estimation of the full set of target parameters (*i.e.*, ratios of the moments of inertia, position and location of the principal axes reference frame). It therefore inherits the continuous-discrete formulation, the dual error quaternion concept, and the use of the vector part of the quaternion as three-parameter attitude representation from the kinematic-only DQ MEKF of Filipe et al. (2015). As for the dynamics, instead, the DQ formulation of the equations of the 6 DoF relative motion are used. Differently from Hou et al. (2017), where the absolute dynamics was employed, this provides a consistent formulation in the relative variables. This aspect eases the physical insight for CPO applications and minimizes the impacts of numerical issues related to the DQ algebra. As for the measurement equation, two formulations are proposed, depending on whether each observation is expressed as the couple of quaternion and relative displacement or as the pose *unit* dual quaternion. In this latter case it is demonstrated that the propagation of the measurement errors through the nonlinear definition of the pose unit DQ produces negligible effects. Accordingly, a constant definition of the measurement covariance matrix can be employed in both formulations. Finally, the constant parameters defining position and orientation of the target principal axes are also cast as a unit DQ variable, unlike the formulation of Gaias and Lovera (2022), where an Aghili and Parsa-like approach has been retained. This aspect makes the whole DQ formulation of the filter consistent and simplifies the expressions of the measurement sensitivity matrices.
2. The implementation of the filtering scheme to deliver state and parameters estimation with a general structure that can be specified to address a wide range of design possibilities for the architecture of the close-range navigation system. This has been made possible by writing the measurement equation for a generic point of the target s/c and by expressing it into a convenient reference frame to simplify its expression as function of the filter general state. The availability of a general filtering scheme allows simplifying structure and interfaces of the GNC system, since the same filter unit can be used

as backbone of different GNC modes. Moreover, this fosters the flexibility of the navigation system, since a refinement of the parameters becomes possible in multiple phases of the CPOs. At the same time, if required by specific situations (*e.g.*, poor identifiability of the parameters due to very low angular rate) the filter settings may be tuned to reduce the number of parameters effectively estimated. This is easily obtained for example by adjusting the initial covariance values associated to the initial guess of the filter. To show the flexibility of the proposed approach, the paper provides the expressions that the main design variables take in four possible applications that span from loosely- to tightly-coupled architecture solutions. For each of the provided examples, numerical simulations are carried out to show the behavior of the filter within a scenario representative of close-range target inspection at conclusion of the mid-range rendezvous.

After this introduction, the paper is structured as follows.

Section 2, after a brief mathematical background necessary to derive the developments of the paper, recalls the DQ representations of absolute/relative 6 DoF kinematics and rigid body dynamics. These latter are compared to their classical counterparts. Section 3 first introduces reference systems and definitions to characterize the close-range CPOs scenario. Afterwards, it presents in detail the core general structure of the MEKF for 6 DoF state and parameters' estimation of noncooperative targets. Section 4 lists possible specific applications of the filter when dealing with different architectures of the relative navigation system. Finally, prior to Conclusions, Section 5 provides a set of numerical simulations associated with the specific cases previously introduced.

2. Coupled 6-DoF relative motion

This section describes the model of the coupled rotational-translational relative motion that constitutes the backbone of the subsequent filter design. The attitude is parametrized in unit quaternions, following the most widely used approach in attitude estimation (Crassidis et al., 2007). The pose of a reference frame with respect to another one is written as a unit dual quaternion, whose real part conveys the rotation between the axis whereas the dual part is function of the translation between the origins of the two reference frames (Filipe et al., 2015).

2.1. Mathematical preliminaries

This subsection recalls definition and main properties of quaternions and dual quaternions, which are essential for deriving the results presented in this work. For additional details on quaternions and dual quaternions algebra, the Reader is referred to Filipe et al. (2015); Filipe and Tsiotras (2015); Filipe and Tsiotras (2013b).

2.1.1. Quaternions

In this work a quaternion is represented as the ordered pair $q = (q_0, \bar{q})$, where $q_0 \in \mathbb{R}$ and $\bar{q} = [q_1\, q_2\, q_3]^{\mathrm{T}} \in \mathbb{R}^3$ are respectively *scalar* and *vector* part of the quaternion defined as $q = q_0 + q_1 i + q_2 j + q_3 k$ with $q_0, q_1, q_2, q_3 \in \mathbb{R}$ and i, j, k satisfying $i^2 = j^2 = k^2 = -1$, $i = jk = -kj$, $j = ki = -ik$, and $k = ij = -ji$ (Filipe et al., 2015). *Vector quaternions* are quaternions with zero scalar part $(0, \bar{q})$; whereas *scalar quaternions* are quaternions with zero vector part $(q_0, \bar{0})$, with $\bar{0} = 0_{3\times 1}$. The sets of quaternions, vector quaternions, and scalar quaternions are denoted respectively, by $\mathbb{H} = \{q : q = q_0 + q_1 i + q_2 j + q_3 k, q_0, \quad q_1, q_2, q_3 \in \mathbb{R}\}$, $\mathbb{H}^v = \{q \in \mathbb{H} : q_0 = 0\}$, and $\mathbb{H}^s = \{q \in \mathbb{H} : q_1 = q_2 = q_3 = 0\}$. Identity and null quaternions are denoted by $\mathbf{1} = (1, \bar{0})$ and $\mathbf{0} = (0, \bar{0})$, respectively. The definitions of the basic operations between quaternions are reported in Table 1, where $a, b \in \mathbb{H}$ and $\lambda \in \mathbb{R}$.

The multiplication of a 4-by-4 matrix with a quaternion is defined as $\mathrm{M} * q = (\mathrm{M}_{11} q_0 + \mathrm{M}_{12}\bar{q}, \mathrm{M}_{21} q_0 + \mathrm{M}_{22}\bar{q})$ with $\mathrm{M}_{11} \in \mathbb{R}, \mathrm{M}_{12} \in \mathbb{R}^{1\times 3}, \mathrm{M}_{21} \in \mathbb{R}^{3\times 1}$, and $\mathrm{M}_{22} \in \mathbb{R}^{3\times 3}$ (Filipe and Tsiotras, 2013b). The bijective mapping between the set of quaternions and $\mathbb{R}^4$ is denoted by $[\cdot]\ \mathbb{H} \to \mathbb{R}^4$, where $[q] = [q_0\, q_1\, q_2\, q_3]^{\mathrm{T}}$.

A *unit* quaternion is defined as a quaternion that belongs to the set $\mathbb{H}^u = \{q \in \mathbb{H} : q \cdot q = qq^* = q^* q = \mathbf{1}\}$. The orientation of the frame $\{\mathrm{Y}\}$ with respect to $\{\mathrm{X}\}$ can be expressed by the unit quaternion $q_{\mathrm{YX}} = \left(\cos\left(\frac{\phi}{2}\right), \sin\left(\frac{\phi}{2}\right)\bar{n}\right)$ which conveys the rotation from $\{\mathrm{X}\}$ to $\{\mathrm{Y}\}$, with $\bar{n}$ and ϕ Euler axis and angle of the rotation. For $-180 < \phi < 180$ deg, the scalar part of the unit quaternion is given by:

$$q_{\mathrm{YX},0} = \sqrt{1 - \|\bar{q}_{\mathrm{YX}}\|^2}. \tag{1}$$

The coordinates of a vector $\bar{v}$ can be transformed from one to the other system through:

$$v^{\mathrm{Y}} = q^*_{\mathrm{YX}}\, v^{\mathrm{X}}\, q_{\mathrm{YX}} \qquad v^{\mathrm{X}} = q_{\mathrm{YX}}\, v^{\mathrm{Y}}\, q^*_{\mathrm{YX}} \tag{2}$$

where $v^{\mathrm{X}} = (0, \bar{v}^{\mathrm{X}}) \in \mathbb{H}^v$ is the vector quaternion from $\bar{v}$ written in $\{\mathrm{X}\}$.

2.1.2. Dual quaternions

A dual quaternion is represented as $\hat{q} = q_r + \epsilon q_d$, where ϵ is the dual unit defined by $\epsilon^2 = 0$ and $\epsilon \neq 0$, whereas q_r and q_d are respectively the *real part* and *dual part* quaternions. A *dual vector quaternion* is formed from vector quaternions as $(0, \bar{q}_r) + \epsilon(0, \bar{q}_d)$; whereas a *dual scalar quaternion* is formed from scalar quaternions as $(q_{r0}, \bar{0}) + \epsilon(q_{d0}, \bar{0})$. The sets of dual quaternions, dual vector quaternions, and dual scalar quaternions are denoted respectively by $\mathbb{H}_d = \{\hat{q} : \hat{q} = (q_r + \epsilon q_d), q_r, q_d \in \mathbb{H}\}$, $\mathbb{H}^v_d = \{\hat{q} : \hat{q} = (q_r + \epsilon q_d), q_r, q_d \in \mathbb{H}^v\}$, and $\mathbb{H}^s_d = \{\hat{q} : \hat{q} = (q_r + \epsilon q_d), q_r, q_d \in \mathbb{H}^s\}$. Identity and null dual quaternions are denoted by $\hat{\mathbf{1}} = \mathbf{1} + \epsilon\mathbf{0}$ and

Table 1
Basic operations between quaternions.

Operation	Definition	Belonging to
Addition	$a+b=(a_0+b_0,\bar{a}+\bar{b})$	$\in\mathbb{H}$
Multiplication by a scalar	$\lambda a=(\lambda a_0+,\lambda\bar{a})$	$\in\mathbb{H}$
Multiplication	$ab=(a_0b_0-\bar{a}\cdot\bar{b},a_0\bar{b}+b_0\bar{a}+\bar{a}\times\bar{b})$	$\in\mathbb{H}$
Conjugation	$a^*=(a_0,-\bar{a})$	$\in\mathbb{H}$
Dot product	$a\cdot b=(a_0b_0+\bar{a}\cdot\bar{b},\bar{0})$	$\in\mathbb{H}^s$
Cross product	$a\times b=(0,b_0\bar{a}+a_0\bar{b}+\bar{a}\times\bar{b})$	$\in\mathbb{H}^v$
Norm	$\|a\|^2=a\cdot a=aa^*=a^*a$	$\in\mathbb{H}^s$

$\hat{\mathbf{0}}=\mathbf{0}+\epsilon\mathbf{0}$, respectively. The basic operations between dual quaternions are recalled in Table 2, where $\hat{a},\hat{b}\in\mathbb{H}_d$.

The multiplication of a 8-by-8 matrix with a dual quaternion is defined as $\mathbf{M}\bigstar\hat{q}=(\mathbf{M}_{11}*q_r+\mathbf{M}_{12}*q_d)+\epsilon(\mathbf{M}_{21}*q_r+\mathbf{M}_{22}*q_d)$, with $\mathbf{M}_{11},\mathbf{M}_{12},\mathbf{M}_{21},\mathbf{M}_{22}\in\mathbb{R}^{4\times4}$ (Filipe and Tsiotras, 2013b). The bijective mapping between the set of dual quaternions and $\mathbb{R}^8$ is denoted by $[\cdot]\ \mathbb{H}_d\rightarrow\mathbb{R}^8$, where $[\hat{q}]=\left[[q_r]^{\mathrm{T}}\,[q_d]^{\mathrm{T}}\right]^{\mathrm{T}}$. The operator $\bar{\cdot}\ \mathbb{H}_d\rightarrow\mathbb{R}^6$ so that $\bar{\hat{q}}=\left[[\bar{q}_r]^{\mathrm{T}}\,[\bar{q}_d]^{\mathrm{T}}\right]^{\mathrm{T}}$ is introduced to extract the vector parts from both real and dual parts.

A *unit* dual quaternion is defined as a dual quaternion that belongs to the set $\mathbb{H}_d^u=\{\hat{q}\in\mathbb{H}:q_r\cdot q_r=\mathbf{1}\text{ and }q_r\cdot q_d=\mathbf{0}\}$. Considering two reference systems $\{\mathrm{Y}\}$ and $\{\mathrm{X}\}$, such that the origin of $\{\mathrm{Y}\}$ is translated by $\bar{r}_{\mathrm{YX}}$ with respect to the origin of $\{\mathrm{X}\}$ and the attitude of $\{\mathrm{Y}\}$ with respect to $\{\mathrm{X}\}$ is given by the unit quaternion q_{YX}, the *pose* of a reference system $\{\mathrm{Y}\}$ with respect to $\{\mathrm{X}\}$ can be expressed by the *unit* dual quaternion $\hat{q}_{\mathrm{YX}}$ (read from $\{\mathrm{X}\}$ to $\{\mathrm{Y}\}$):

$$\begin{aligned}\hat{q}_{\mathrm{YX}}&=q_{\mathrm{YX,r}}+\epsilon q_{\mathrm{YX},d}=q_{\mathrm{YX}}+\epsilon\frac{1}{2}r^{\mathrm{X}}_{\mathrm{YX}}q_{\mathrm{YX}}\\&=q_{\mathrm{YX}}+\epsilon\frac{1}{2}q_{\mathrm{YX}}r^{\mathrm{Y}}_{\mathrm{YX}}\end{aligned}\tag{3}$$

where the real part is the unit quaternion q_{YX}, and the dual part is defined differently if the translation between the origins is written in $\{\mathrm{X}\}$ or in $\{\mathrm{Y}\}$. The quantity $\bar{r}_{\mathrm{YX}}$ conveys the distance between the points Y and X, which denote the origins of the corresponding reference systems, taken as the vector Y-X. Since $\hat{q}_{\mathrm{YX}}\in\mathbb{H}_d^u$, the scalar part of the dual quaternion can be computed as:

$$q_{\mathrm{YX},d,0}=\frac{-\bar{q}^{\mathrm{T}}_{\mathrm{YX}}\bar{q}_{\mathrm{YX},d}}{q_{\mathrm{YX},0}}\,.\tag{4}$$

The translation between the origins is extracted from the unit dual quaternion through:

$$r^{\mathrm{X}}_{\mathrm{YX}}=2q_{\mathrm{YX},d}q^*_{\mathrm{YX}}\qquad r^{\mathrm{Y}}_{\mathrm{YX}}=2q^*_{\mathrm{YX}}q_{\mathrm{YX},d}\tag{5}$$

which are linear in q_{YX}. The change of reference system for a dual quaternion quantity $\hat{w}$ is performed through:

$$\hat{w}^{\mathrm{Y}}=\hat{q}^*_{\mathrm{YX}}\hat{w}^{\mathrm{X}}\hat{q}_{\mathrm{YX}}\qquad\hat{w}^{\mathrm{X}}=\hat{q}_{\mathrm{YX}}\hat{w}^{\mathrm{Y}}\hat{q}^*_{\mathrm{YX}}\,.\tag{6}$$

2.2. Dual quaternion representation of the rotational and translational kinematic equations

The rotational and translational kinematic equations of the motion of the $\{\mathrm{Y}\}$ frame with respect to the $\{\mathrm{X}\}$ one can be written compactly in terms of dual quaternions as Wu et al. (2005, 2015):

$$\frac{d}{dt}\hat{q}_{\mathrm{YX}}=\dot{\hat{q}}_{\mathrm{YX}}=\frac{1}{2}\hat{\omega}^{\mathrm{X}}_{\mathrm{YX}}\hat{q}_{\mathrm{YX}}=\frac{1}{2}\hat{q}_{\mathrm{YX}}\hat{\omega}^{\mathrm{Y}}_{\mathrm{YX}}\tag{7}$$

where $\hat{\omega}^{\mathrm{Z}}_{\mathrm{YX}}\in\mathbb{H}_d^v$ is the dual velocity of Y w.r.t $\{\mathrm{X}\}$ written in the frame $\{\mathrm{Z}\}$. The components of $\hat{\omega}^{\mathrm{Z}}_{\mathrm{YX}}$ are defined differently, depending on whether the frames are moving or not. By considering an inertial frame $\{\mathrm{I}\}$ and a body-fixed frame $\{\mathrm{B}\}$ attached to a spacecraft, the dual velocity in $\{\mathrm{I}\}$ is expressed as:

$$\hat{\omega}^{\mathrm{I}}_{\mathrm{BI}}=\omega^{\mathrm{I}}_{\mathrm{BI}}+\epsilon\left(\dot{r}^{\mathrm{I}}_{\mathrm{BI}}+r^{\mathrm{I}}_{\mathrm{BI}}\times\omega^{\mathrm{I}}_{\mathrm{BI}}\right)\tag{8}$$

where the real part $\omega^{\mathrm{I}}_{\mathrm{BI}}$ is the angular rate of the body w.r.t. $\{\mathrm{I}\}$, written in $\{\mathrm{I}\}$. In the dual part, the quantity $\dot{r}^{\mathrm{I}}_{\mathrm{BI}}$ is equal to the absolute linear velocity $v^{\mathrm{I}}_{\mathrm{BI}}$, since $\{\mathrm{I}\}$ is an iner-

Table 2
Basic operations between dual quaternions.

Operation	Definition	Belonging to
Addition	$\hat{a}+\hat{b}=(a_r+b_r)+\epsilon(a_d+b_d)$	$\in\mathbb{H}_d$
Multiplication by a scalar	$\lambda\hat{a}=(\lambda a_r)+\epsilon(\lambda a_d)$	$\in\mathbb{H}_d$
Multiplication	$\hat{a}\hat{b}=(a_rb_r)+\epsilon(a_rb_d+a_db_r)$	$\in\mathbb{H}_d$
Conjugation	$\hat{a}^*=a_r^*+\epsilon a_d^*$	$\in\mathbb{H}_d$
Dot product	$\hat{a}\cdot\hat{b}=(a_r\cdot b_r)+\epsilon(a_d\cdot b_r+a_r\cdot b_d)$	$\in\mathbb{H}_d^s$
Cross product	$\hat{a}\times\hat{b}=(a_r\times b_r)+\epsilon(a_d\times b_r+a_r\times b_d)$	$\in\mathbb{H}_d^v$
Norm	$\|\hat{a}\|^2=\hat{a}\cdot\hat{a}=\hat{a}\hat{a}^*=\hat{a}^*\hat{a}$	$\in\mathbb{H}_d^s$
Swap	$\hat{a}^{\mathrm{s}}=a_d+\epsilon a_r$	$\in\mathbb{H}_d$

tial frame. The dual velocity in {B} is computed from $\hat{\omega}^{\mathrm{I}}_{\mathrm{BI}}$ using Eq. (6), to obtain:

$$\hat{\omega}^{\mathrm{B}}_{\mathrm{BI}} = \omega^{\mathrm{B}}_{\mathrm{BI}} + \epsilon\left(v^{\mathrm{B}}_{\mathrm{BI}} - r^{\mathrm{B}}_{\mathrm{BI}} \times \omega^{\mathrm{B}}_{\mathrm{BI}}\right) = \omega^{\mathrm{B}}_{\mathrm{BI}} + \epsilon\dot{r}^{\mathrm{B}}_{\mathrm{BI}} \tag{9}$$

As for the dual part, the former version is function of the absolute linear velocity of the point B written in {B} (Wu et al., 2005), the latter version is function of the component $\dot{r}^{\mathrm{B}}_{\mathrm{BI}}$ relative to the frame {B} (Filipe et al., 2015), since in the moving frame $v^{\mathrm{B}}_{\mathrm{BI}} = \dot{r}^{\mathrm{B}}_{\mathrm{BI}} - \omega^{\mathrm{B}}_{\mathrm{BI}} \times r^{\mathrm{B}}_{\mathrm{BI}}$. The derivation of Eq. (7) is demonstrated in Appendix C of Wu et al. (2005), making use of Plücker lines.

By introducing a further reference system {D} attached to a second spacecraft, it holds:

$$\hat{q}_{\mathrm{BD}} = \hat{q}^{*}_{\mathrm{DI}}\hat{q}_{\mathrm{BI}} = q_{\mathrm{BD}} + \epsilon\frac{1}{2}q_{\mathrm{BD}}r^{\mathrm{B}}_{\mathrm{BD}} = q_{\mathrm{BD}} + \epsilon\frac{1}{2}r^{\mathrm{D}}_{\mathrm{BD}}q_{\mathrm{BD}} \tag{10}$$

and the *relative* dual velocity $\hat{\omega}^{\mathrm{B}}_{\mathrm{BD}} \in \mathbb{H}^{v}_{d}$ is given by:

$$\begin{aligned}\hat{\omega}^{\mathrm{B}}_{\mathrm{BD}} &= \omega^{\mathrm{B}}_{\mathrm{BD}} + \epsilon\left(\dot{r}^{\mathrm{B}}_{\mathrm{BI}} - \dot{r}^{\mathrm{B}}_{\mathrm{DI}} - \omega^{\mathrm{B}}_{\mathrm{DI}} \times r^{\mathrm{B}}_{\mathrm{BD}}\right)\\ &= \omega^{\mathrm{B}}_{\mathrm{BD}} + \epsilon\dot{\rho}^{\mathrm{B}},\end{aligned} \tag{11}$$

which can also be written as $\hat{\omega}^{\mathrm{B}}_{\mathrm{BD}} = \hat{\omega}^{\mathrm{B}}_{\mathrm{BI}} - \hat{\omega}^{\mathrm{B}}_{\mathrm{DI}}$ and has the relative angular rate between the bodies ω_{BD} in the real part and the relative linear velocity $\dot{\rho}$ in the dual part. The relative dual velocity $\hat{\omega}^{\mathrm{D}}_{\mathrm{BD}}$ can be computed from Eq. (11) and $\hat{q}_{\mathrm{BD}}$ using Eq. (6). Note that Eq. (7) is formally equivalent to the quaternion-based rotation-only kinematic equation. Moreover, no hypothesis on the origin and axes orientation of the moving frames have been introduced so far.

2.3. Dual quaternion representation of the rigid body dynamic equations

The 6 DoF equations of the rigid body dynamics of a satellite are given by (Filipe and Tsiotras, 2013c):

$$\mathrm{M}_{\mathrm{B}}\bigstar\left(\dot{\hat{\omega}}^{\mathrm{B}}_{\mathrm{BI}}\right)^{\mathrm{s}} = \hat{f}^{\mathrm{B}}_{\mathrm{B}} - \hat{\omega}^{\mathrm{B}}_{\mathrm{BI}} \times \left(\mathrm{M}_{\mathrm{B}}\bigstar\left(\hat{\omega}^{\mathrm{B}}_{\mathrm{BI}}\right)^{\mathrm{s}}\right) \tag{12}$$

where now {B} denotes the body-fixed reference frame with origin in the center of mass B of the satellite. The term $\hat{f}^{\mathrm{B}}_{\mathrm{B}} \in \mathbb{H}^{v}_{d}$ is the *dual force* applied to the spacecraft about its center of mass B written in {B}. This is a dual vector quaternion with parts $f^{\mathrm{B}}_{\mathrm{B},r} = \left(0, \bar{f}^{\mathrm{B}}_{\mathrm{B}}\right)$ and $f^{\mathrm{B}}_{\mathrm{B},d} = \left(0, \bar{\tau}^{\mathrm{B}}_{\mathrm{B}}\right)$, with $\bar{f}^{\mathrm{B}}_{\mathrm{B}}$ total external force vector applied to the satellite and $\bar{\tau}^{\mathrm{B}}_{\mathrm{B}}$ total external moment vector applied to the spacecraft about its center of mass. The quantity M_{B} is termed *dual inertia matrix* and defined as:

$$\mathrm{M}_{\mathrm{B}} = \begin{bmatrix} 1 & 0_{1\times 3} & 0 & 0_{1\times 3} \\ 0_{3\times 1} & m_{\mathrm{B}}\mathrm{I}_3 & 0_{3\times 1} & 0_{3\times 3} \\ 0 & 0_{1\times 3} & 1 & 0_{1\times 3} \\ 0_{3\times 1} & 0_{3\times 3} & 0_{3\times 1} & \bar{\mathrm{I}}_{\mathrm{B}} \end{bmatrix} \tag{13}$$

where m_{B} is the mass of the satellite, $0_{i\times j}$ is the zero matrix of size $i \times j$, I_n the identity matrix of dimension n, and $\bar{\mathrm{I}}_{\mathrm{B}}$ the mass moment of inertia of the satellite about its center of mass B written in the frame {B}. As explained in Filipe and Tsiotras (2013c), the definition of the symmetric matrix of Eq. (13) allows to compute the inverse of M_{B} as $(\mathrm{M}_{\mathrm{B}})^{-1}$ and supports the ★ multiplication between 8×8 matrices and dual quaternions. The meaning of Eq. (12) becomes evident by carrying out the dual quaternion operations. For the vector part of the real quaternion one obtains:

$$\bar{\ddot{r}}^{\mathrm{B}}_{\mathrm{BI}} = \frac{1}{m_{\mathrm{B}}}\bar{f}^{\mathrm{B}}_{\mathrm{B}} \tag{14}$$

which is the translational dynamics of a rigid body relative to moving body-frame {B} (Wang and Yu, 2010). For the vector part of the dual quaternion one obtains:

$$\bar{\dot{\omega}}^{\mathrm{B}}_{\mathrm{BI}} = \bar{\mathrm{I}}^{-1}_{\mathrm{B}}\bar{\tau}^{\mathrm{B}}_{\mathrm{B}} - \bar{\mathrm{I}}^{-1}_{\mathrm{B}}\left(\bar{\omega}^{\mathrm{B}}_{\mathrm{BI}} \times \bar{\mathrm{I}}_{\mathrm{B}}\bar{\omega}^{\mathrm{B}}_{\mathrm{BI}}\right) \tag{15}$$

which are the Euler equations for the rotational dynamics.

2.4. Dual quaternion representation of the relative dynamic equations

The 6 DoF equations of the relative dynamics between two satellites are given by (Filipe and Tsiotras, 2013b):

$$\begin{aligned}\left(\dot{\hat{\omega}}^{\mathrm{B}}_{\mathrm{BD}}\right)^{\mathrm{s}} = \mathrm{M}^{-1}_{\mathrm{B}}\bigstar\Big[\hat{f}^{\mathrm{B}}_{\mathrm{B}} - \left(\hat{\omega}^{\mathrm{B}}_{\mathrm{BD}} + \hat{\omega}^{\mathrm{B}}_{\mathrm{DI}}\right) \times \left(\mathrm{M}_{\mathrm{B}}\bigstar\left(\hat{\omega}^{\mathrm{B}}_{\mathrm{BD}} + \hat{\omega}^{\mathrm{B}}_{\mathrm{DI}}\right)^{\mathrm{s}}\right)\Big]\\ - \left(\hat{q}^{*}_{\mathrm{BD}}\dot{\hat{\omega}}^{\mathrm{D}}_{\mathrm{DI}}\hat{q}_{\mathrm{BD}}\right)^{\mathrm{s}} - \left(\hat{\omega}^{\mathrm{B}}_{\mathrm{DI}} \times \hat{\omega}^{\mathrm{B}}_{\mathrm{BD}}\right)^{\mathrm{s}}\end{aligned} \tag{16}$$

where {D} denotes the body-fixed reference frame with origin in the center of mass D of the second satellite. This is derived from the difference of the absolute dynamics of both satellites $\left(\dot{\hat{\omega}}^{\mathrm{B}}_{\mathrm{BD}}\right)^{\mathrm{s}} = \left(\dot{\hat{\omega}}^{\mathrm{B}}_{\mathrm{BI}}\right)^{\mathrm{s}} - \left(\dot{\hat{\omega}}^{\mathrm{B}}_{\mathrm{DI}}\right)^{\mathrm{s}}$, noting that the swap of the addition is equal to the addition of the swaps. Moreover, to derive Eq. (16) the dual quaternion counterpart to the classical transport theorem (see Proposition 1 of Filipe and Tsiotras (2013b)) is used to compute the time derivative of $\hat{v}^{\mathrm{Y}} \in \mathbb{H}^{v}_{d}$ known such derivative of the dual vector quaternion in {X}:

$$\dot{\hat{v}}^{\mathrm{Y}} = \hat{q}^{*}_{\mathrm{YX}}\left(\dot{\hat{v}}^{\mathrm{X}} - \hat{\omega}^{\mathrm{X}}_{\mathrm{YX}} \times \hat{v}^{\mathrm{X}}\right)\hat{q}_{\mathrm{YX}}. \tag{17}$$

Formally, Eq. (16) is equivalent to the quaternion-based rotation-only relative dynamics (*e.g.*, see Eq. (5) of Filipe and Tsiotras (2013a) or Eq. (19) of Segal and Gurfil (2009) to the net of one rotation, since this is written in {D} instead of in {B}). This is obvious for the dual part, since the real part of the relative dual velocity is the relative angular rate. As for the real part of Eq. (16), by carrying out the dual quaternion operations one obtains:

$$\bar{\ddot{r}}^{\mathrm{B}}_{\mathrm{BD}} = \frac{1}{m_{\mathrm{B}}}\bar{f}^{\mathrm{B}}_{\mathrm{B}} - \frac{1}{m_{\mathrm{D}}}\bar{f}^{\mathrm{B}}_{\mathrm{D}} \tag{18}$$

which is the difference of the absolute translational dynamics of the two spacecraft written in the moving frame {B}. Whereas, if the operations are performed keeping the terms function of $\bar{\dot{\rho}}^{\mathrm{B}}$, the following equations are obtained:

$$\begin{aligned}\ddot{\bar{\rho}}^{\mathrm{B}} &= \bar{a}^{\mathrm{B}}_{\mathrm{BD}} + \left(\bar{\omega}^{\mathrm{B}}_{\mathrm{DI}} \times \bar{r}^{\mathrm{B}}_{\mathrm{BD}}\right) \times \bar{\omega}^{\mathrm{B}}_{\mathrm{DI}} + \\ &+ \bar{r}^{\mathrm{B}}_{\mathrm{BD}} \times \dot{\bar{\omega}}^{\mathrm{B}}_{\mathrm{DI}} - 2\bar{\omega}^{\mathrm{B}}_{\mathrm{DI}} \times \dot{\bar{\rho}} + \ddot{\bar{\rho}} \times \bar{\omega}^{\mathrm{B}}_{\mathrm{BD}}\end{aligned} \tag{19}$$

where $\bar{a}^{\mathrm{B}}_{\mathrm{BD}}$ is the acceleration due to the total relative external forces. Eq. (19) is equivalent to Eq. (4) of Cao and Misra (2015), to the net of the rotation necessary to express it in {B}: the last term of Eq. (19) is the transport contribution when writing the relative dynamics of the body B w.r.t the satellite D (*i.e.*, B-D) though expressed in the moving frame {B}.

3. Noncooperative spacecraft pose and parameters estimation in loosely- and tightly-coupled navigation systems

This section introduces the space segment during proximity operations to perform close-range navigation around a noncooperative target satellite. Afterwards, it describes the core structure of a multiplicative extended Kalman filter using dual quaternions to perform pose and parameters estimation of the target satellite.

3.1. Reference systems and navigation system's architectures

The space segment during CPOs is composed of a chaser satellite and a target object flying into two neighboring orbits. The chaser is equipped with a relative navigation system to observe and estimate the relative state of the target spacecraft with respect to itself. In order to support safe operations, which involve the prediction of the motion of the target object, an accurate knowledge of the 6 DoF relative state is required in real-time.

The following reference systems are introduced: {I} the inertial reference system taken as the Earth mean equator and equinox (EME) of J2000 with origin denoted by I; {D} a chaser body-fixed reference with origin D in its center of mass and axes oriented as the chaser principal axes; {B} a target body-fixed reference with origin B in its center of mass and axes oriented as the target principal axes; {G} a target body-fixed reference with origin G in the geometrical center of the spacecraft and axes arbitrarily defined.

Fig. 1 a) depicts how the pose unit dual quaternions relate to each other (*e.g.*, $\hat{q}_{\mathrm{BD}}$ as in Eq. (10) and $\hat{q}_{\mathrm{GD}} = \hat{q}_{\mathrm{BD}}\hat{q}_{\mathrm{GB}}$). Dashed connectors denote unit DQs that are function of time, $\hat{q}_{\mathrm{GB}}$ is constant within the hypothesis of rigid body of the target. Without loss of generality, the frame of the relative navigation sensor on the chaser is assumed coincident with {D}, since both mounting position and orientation on the chaser are assumed known or calibrated accurately. Fig. 1 b) focuses on the relationship between principal and geometrical axes of the target satellite. Accordingly, the coordinates of a generic feature P_i on the target are given by: $\bar{r}^{\mathrm{B}}_{\mathrm{P}_i\mathrm{B}} = \bar{r}^{\mathrm{B}}_{\mathrm{P}_i\mathrm{G}} + \bar{r}^{\mathrm{B}}_{\mathrm{GB}}$. Following the assumption of rigid body, all the parameters of the target are constant quantities. Moreover, without loss of generality, all the arbitrary frames associated with each detected feature P_i are oriented as the geometric reference frame (*i.e.*, $q_{\mathrm{P}_i\mathrm{B}} = q_{\mathrm{GB}}$).

To date, the proposed architectures of close-range navigation systems present either a tightly-coupled or loosely-coupled structure (Opromolla et al., 2017; Pasqualetto Cassinis et al., 2019; Pasqualetto Cassinis et al., 2021). The first option combines the sensor data processing and the filtering task into a single functional block. The loosely-coupled option splits the pose estimation and the filtering scheme in two separate sequential blocks. Accordingly, the pose estimation algorithm provides a set of pseudo-measurements to the update step of the filter. In order to perform pose determination of noncooperative targets, electro-optical sensing devices are usually employed given their mass and power consumption features (Opromolla et al., 2017). These devices these collect the radiations reflected and/or directly emitted by the target in the optical spectrum. Depending on the specific technology used, examples of possible sensor outputs are the 3D data sets gathering multiple echoes coming from an assigned field of view or the pixel coordinates on an image corresponding to a feature detected on the target. Since this work focuses on the filtering scheme, the data collected by the sensors are assumed as the measurements expressing the relative quaternion and displacement between a point

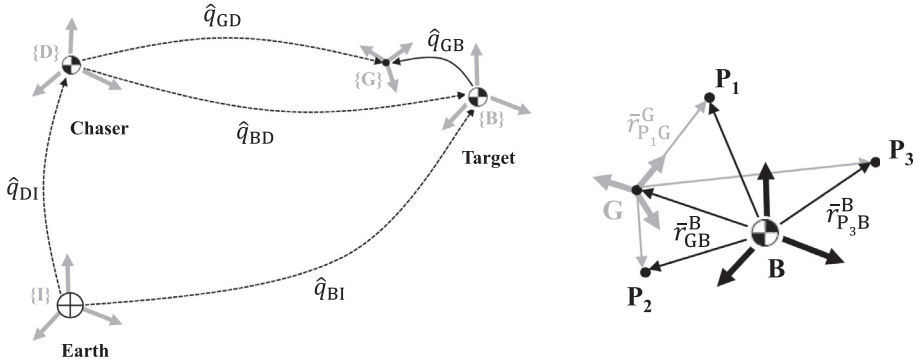

a) Relationship among unit dual quaternions.

b) Relationship between the origins of target geometric and principal frames.

Fig. 1. Reference systems during CPOs.

of the target and {D}. Accordingly, for tightly-coupled configurations, an additional relation between the technology-dependent expression of the observations and the quaternion-displacement measurements is generally required (*e.g.*, for example using the perspective-n-points equations if vision-based image processing is regarded (Pasqualetto Cassinis et al., 2021)).

Fig. 2 summarizes the possible sets of the variables to be estimated, depending on the architecture of the navigation system in use. Note that the state $\xi^{(3)}$ embodies the most general formulation for the loosely-coupled case as well as the simplest formulation of tightly-coupled problems, where only one feature is detected. The considered sets are composed of the subset of variables that express the 6 DoF relative state, namely: the unit dual quaternion of the relative pose $\hat{q}_{\mathrm{BD}}$ and the dual vector quaternion of the relative dual velocity $\hat{\omega}^{\mathrm{B}}_{\mathrm{BD}}$. The second subset comprises the collection of the additional target parameters to be estimated. Here, $\bar{p}^{\mathrm{B}}$ denotes the vector of the inertia ratios of the target so defined:

$$\begin{aligned} \bar{p}_{\mathrm{B}} &= \begin{bmatrix} p_x & p_y & p_z \end{bmatrix}^{\mathrm{T}} \in \mathbb{R}^3 \\ p_x = \tfrac{I_{yy}-I_{zz}}{I_{xx}}, p_y &= \tfrac{I_{zz}-I_{xx}}{I_{yy}}, p_z = \tfrac{I_{xx}-I_{yy}}{I_{zz}} \end{aligned} \tag{20}$$

with I_{ii} principal moment of inertia of the target w.r.t. the i axis. As it is well known the principal moments of inertia are not structurally identifiable from torque-free motion measurements alone. For this reason the inertia ratios will be considered as parameters to be estimated (Aghili and Parsa, 2009; Sheinfeld and Rock, 2009). The quantities $\hat{q}_{\mathrm{GB}}$ and $\hat{q}_{\mathrm{P}_i\mathrm{B}}$ convey the pose of the geometric frames, either with origin in G or P_i, w.r.t. {B}. Finally, the quantities $\bar{r}^{\mathrm{B}}_{\mathrm{P}_i\mathrm{B}}$ express the coordinates of the generic feature P_i written in {B}. Further details on how the variables' sets relate to the architecture of the navigation system are provided later in Section 4.

3.2. Dual quaternion multiplicative extended Kalman filter

This section describes the core structure common to all the filters that estimate the states listed in Fig. 2. The general filter is designed as a MEKF in the continuous time domain using dual quaternions. The foundation is inherited from the dual quaternion based kinematic MEKF of Filipe et al. (2015). Though here it is enhanced by including the relative dynamics, which enables dynamic filtering and parameters estimation.

The full state of the system is defined as:

$$\xi_v(t) = \begin{bmatrix} [\hat{q}_{\mathrm{BD}}]^{\mathrm{T}} & [\hat{\omega}^{\mathrm{B}}_{\mathrm{BD}}]^{\mathrm{T}} & s^{\mathrm{B}\mathrm{T}} \end{bmatrix}^{\mathrm{T}} \in \mathbb{R}^v \tag{21}$$

where $s^{\mathrm{B}\mathrm{T}}$ denotes a generic collection of constant parameters of the target to be estimated. In the quaternion MEKF framework, the concept of *error quaternion* is introduced to cope with the singularity problems of minimum-parameter representations of the attitude. The quaternion MEKF performs an unconstrained estimate of a three-component error quaternion, while using a correctly normalized four-component reference quaternion to retrieve the global non-singular attitude estimate (Markley, 2003). The *dual error quaternion* is defined in analogy to the error quaternion as (Markley, 2003; Filipe et al., 2015):

$$\delta\hat{q}_{\mathrm{BD}} = \tilde{\hat{q}}^{*}_{\mathrm{BD}}\,\hat{q}_{\mathrm{BD}} \tag{22}$$

and represents the roto-translation error from the estimated pose $\tilde{\hat{q}}_{\mathrm{BD}}$ to the *true* one. As performed in Filipe et al. (2015), the vector part of the quaternion is directly chosen as three-component parametrization of the attitude. Accordingly, the state propagated inside the filter becomes:

$$x_n(t) = \begin{bmatrix} \overline{\delta\hat{q}_{\mathrm{BD}}}^{\mathrm{T}} & \overline{\hat{\omega}^{\mathrm{B}}_{\mathrm{BD}}}^{\mathrm{T}} & s^{\mathrm{B}\mathrm{T}} \end{bmatrix}^{\mathrm{T}} \in \mathbb{R}^n \tag{23}$$

with $n \leqslant (v-4)$, having used the $\bar{\cdot}$ operator introduced in Section 2.1.2 to extract the vector quaternions. The filter state evolves according to:

$$\dot{x}_n(t) = f_n(x_n(t), t) + g_{n\times p}(x_n(t), t) w_p(t) \tag{24}$$

where f_n is composed of $\overline{\frac{d}{dt}\delta\hat{q}_{\mathrm{BD}}}, \overline{\frac{d}{dt}\hat{\omega}^{\mathrm{B}}_{\mathrm{BD}}}$ (from Eq. (16)), and $\dot{s}^{\mathrm{B}} = 0_{q\times 1}$. The quantity w_p is the process noise included in the filter design, which is taken as:

$$w_p(t) = \begin{bmatrix} \bar{\epsilon}^{\mathrm{T}}_{\tau} & \bar{\epsilon}^{\mathrm{T}}_{f} & \bar{\epsilon}^{\mathrm{T}}_{s} \end{bmatrix}^{\mathrm{T}}, \bar{\epsilon}_i \in \mathbb{R}^3\ i = \tau, f, \text{ and } \bar{\epsilon}_s \in \mathbb{R}^q \tag{25}$$

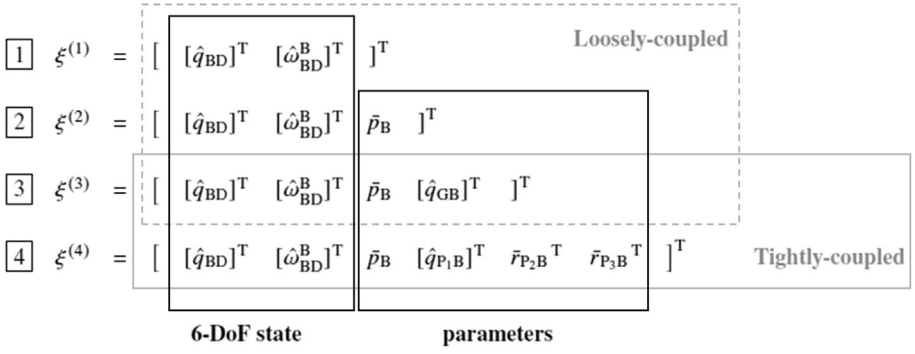

Fig. 2. Possible variable states in relation to the different architectures of the navigation system.

with $\bar{\epsilon}_i$ zero-mean Gaussian white noise process to respectively account for: unmodeled relative disturbance torques ($\bar{\epsilon}_\tau$), unmodeled relative disturbance forces ($\bar{\epsilon}_f$), and fictitious noise on the constant parameters ($\bar{\epsilon}_s$). For each process noise component, the covariance is:

$$\mathrm{E}\{\bar{\epsilon}_i(t)\bar{\epsilon}_i^{\mathrm{T}}(\tau)\} = \Sigma_i\delta(t-\tau) \tag{26}$$

with Σ_i either $\in \mathbb{R}^{3\times3}$ or $\in \mathbb{R}^{q\times q}$, symmetric positive defined matrix taken as $\sigma_i^2\mathrm{I}_3$ or $\sigma_i^2\mathrm{I}_q$. The standard deviation values σ_τ, σ_f, and σ_s are tunable parameters of the filter. The overall process noise covariance matrix is then:

$$\Sigma = \mathrm{diag}(\Sigma_\tau, \Sigma_f, \Sigma_s). \tag{27}$$

Following the EKF approximation, the estimated state $\tilde{x}_n(t)$ is propagated through $\dot{\tilde{x}}_n(t) \approx f_n(\tilde{x}_n(t), t)$. And, by defining the state estimation error as $\Delta x_n(t) = x_n(t) - \tilde{x}_n(t)$, the covariance matrix of the state estimation error is given by:

$$P_{n\times n}(t) = \mathrm{E}\{\Delta x_n(t)\Delta x_n^{\mathrm{T}}(\tau)\} \qquad \in \mathbb{R}^{n\times n}. \tag{28}$$

The covariance matrix has to be also propagated in time. Hence, the first-order approximation of the time derivative of the state error Δx is introduced:

$$\frac{d}{dt}\Delta x(t) = \mathrm{F}_{n\times n}(t)\Delta x(t) + \mathrm{G}_{n\times p}(t)w(t) \tag{29}$$

where:

$$\mathrm{F}_{n\times n}(t) \triangleq \left.\frac{\partial f_n(x_n(t),t)}{\partial x_n}\right|_{\tilde{x}_n(t)}, \qquad \mathrm{G}_{n\times p}(t) \triangleq g_{n\times p}(\tilde{x}_n(t),t) \tag{30}$$

with $\mathrm{F}_{n\times n}(t)$ being the Jacobian of f_n evaluated at the current estimate $\tilde{x}_n(t)$, assembled from the linearization of $\overline{\frac{d}{dt}\delta\hat{q}_{\mathrm{BD}}}$ and Eq. (16). $\mathrm{G}_{n\times p}(t)$ introduces the process noise contributions and will be detailed later in Section 4 case by case.

3.2.1. Linearization of the time derivative of the dual error quaternion

The time derivative of the dual error quaternion is written as:

$$\frac{d}{dt}\delta\hat{q}_{\mathrm{BD}} = -\frac{1}{2}\tilde{\hat{\omega}}^{\mathrm{B}}_{\mathrm{BD}}\,\delta\hat{q}_{\mathrm{BD}} + \frac{1}{2}\delta\hat{q}_{\mathrm{BD}}\,\hat{\omega}^{\mathrm{B}}_{\mathrm{BD}} \tag{31}$$

by using the definition of Eq. (22) and the approximation that the estimated dual quaternion evolves in time according to Eq. (7). This latter is the result of the usual EKF technique of approximating the expectation of a nonlinear function (in this case of $\hat{q}$ and $\hat{\omega}$) by the same nonlinear function of their expectations ($\tilde{\hat{q}}$ and $\tilde{\hat{\omega}}$) (Markley, 2003; Filipe et al., 2015). For the sake of conciseness, the following short-hand notation is introduced for the dual error quaternion: $\delta\hat{q}_{\mathrm{BD}} = \delta q + \epsilon\delta\mathrm{B}$ with $\delta q = \delta q_{\mathrm{BD}} = (\delta q_0, \overline{\delta q})$ and $\delta\mathrm{B} = (\delta\mathrm{B}_0, \overline{\delta\mathrm{B}})$. Accordingly, the Jacobian of $\overline{\frac{d}{dt}\delta\hat{q}_{\mathrm{BD}}}$ w.r.t. the 6-DoF relative state part of $x_n(t)$ is denoted by $\mathrm{F}_{\mathrm{kin}}(t) \in \mathbb{R}^{6\times12}$ and computed as:

$$\mathrm{F}_{\mathrm{kin}}(t) \triangleq \left.\begin{bmatrix} \frac{\partial\left(\overline{\frac{d}{dt}\delta\hat{q}_{\mathrm{BD},r}}\right)}{\partial\overline{\delta q}} & \frac{\partial\left(\overline{\frac{d}{dt}\delta\hat{q}_{\mathrm{BD},r}}\right)}{\partial\overline{\delta\mathrm{B}}} & \frac{\partial\left(\overline{\frac{d}{dt}\delta\hat{q}_{\mathrm{BD},r}}\right)}{\partial\omega^{\mathrm{B}}_{\mathrm{BD}}} & \frac{\partial\left(\overline{\frac{d}{dt}\delta\hat{q}_{\mathrm{BD},r}}\right)}{\partial\bar{p}^{\mathrm{B}}} \\ \frac{\partial\left(\overline{\frac{d}{dt}\delta\hat{q}_{\mathrm{BD},d}}\right)}{\partial\overline{\delta q}} & \frac{\partial\left(\overline{\frac{d}{dt}\delta\hat{q}_{\mathrm{BD},d}}\right)}{\partial\overline{\delta\mathrm{B}}} & \frac{\partial\left(\overline{\frac{d}{dt}\delta\hat{q}_{\mathrm{BD},d}}\right)}{\partial\omega^{\mathrm{B}}_{\mathrm{BD}}} & \frac{\partial\left(\overline{\frac{d}{dt}\delta\hat{q}_{\mathrm{BD},d}}\right)}{\partial\bar{p}^{\mathrm{B}}} \end{bmatrix}\right|_{\tilde{\hat{q}}_{\mathrm{BD}},\tilde{\hat{\omega}}^{\mathrm{B}}_{\mathrm{BD}}} \tag{32}$$

which results in:

$$\begin{aligned}\mathrm{F}_{\mathrm{kin}}(t) &= \begin{bmatrix} -\left[\overline{\tilde{\omega}^{\mathrm{B}}_{\mathrm{BD}}}^{\times}\right] & 0_{3\times3} & \frac{1}{2}\delta q_0\mathrm{I}_3 & 0_{3\times3} \\ -\left[\overline{\tilde{\hat{\rho}}^{\mathrm{B}}}^{\times}\right] & -\left[\overline{\tilde{\omega}^{\mathrm{B}}_{\mathrm{BD}}}^{\times}\right] & \frac{1}{2}\delta\mathrm{B}_0\mathrm{I}_3 & \frac{1}{2}\delta q_0\mathrm{I}_3 \end{bmatrix} \\ &\approx \begin{bmatrix} -\left[\overline{\tilde{\omega}^{\mathrm{B}}_{\mathrm{BD}}}^{\times}\right] & 0_{3\times3} & \frac{1}{2}\mathrm{I}_3 & 0_{3\times3} \\ -\left[\overline{\tilde{\hat{\rho}}^{\mathrm{B}}}^{\times}\right] & -\left[\overline{\tilde{\omega}^{\mathrm{B}}_{\mathrm{BD}}}^{\times}\right] & 0_{3\times3} & \frac{1}{2}\mathrm{I}_3 \end{bmatrix}\end{aligned} \tag{33}$$

where $[\bar{a}^{\times}]\bar{b} = \bar{a}\times\bar{b}$. The approximations introduced in Eq. (33) are motivated by the fact that $\delta q_0 \approx 1$ since it is the scalar part of the small error quaternion, whereas $\delta\mathrm{B}_0 = -\frac{1}{2}\overline{\delta r}\cdot\overline{\delta q}$, with $\overline{\delta r} = \bar{r}^{\mathrm{B}}_{\mathrm{BD}} - \tilde{\bar{r}}^{\mathrm{B}}_{\mathrm{BD}}$, is null within the first-order approximation.

3.2.2. Linearization of the relative dynamics equations

The Jacobian of $\overline{\frac{d}{dt}\hat{\omega}^{\mathrm{B}}_{\mathrm{BD}}}$ w.r.t. the 6-DoF relative state and the vector of inertia ratios $\bar{p}_{\mathrm{B}}$ is denoted by $\mathrm{F}_{\mathrm{dyn}}(t) \in \mathbb{R}^{6\times15}$ and computed as:

$$\mathrm{F}_{\mathrm{dyn}}(t) \triangleq \left.\begin{bmatrix} \frac{\partial\left(\overline{\dot{\hat{\omega}}^{\mathrm{B}}_{\mathrm{BD},r}}\right)}{\partial\overline{\delta q}} & \frac{\partial\left(\overline{\dot{\hat{\omega}}^{\mathrm{B}}_{\mathrm{BD},r}}\right)}{\partial\overline{\delta\mathrm{B}}} & \frac{\partial\left(\overline{\dot{\hat{\omega}}^{\mathrm{B}}_{\mathrm{BD},r}}\right)}{\partial\omega^{\mathrm{B}}_{\mathrm{BD}}} & \frac{\partial\left(\overline{\dot{\hat{\omega}}^{\mathrm{B}}_{\mathrm{BD},r}}\right)}{\partial\bar{\hat{\rho}}^{\mathrm{B}}} & \frac{\partial\left(\overline{\dot{\hat{\omega}}^{\mathrm{B}}_{\mathrm{BD},r}}\right)}{\partial\bar{p}_{\mathrm{B}}} \\ \frac{\partial\left(\overline{\dot{\hat{\omega}}^{\mathrm{B}}_{\mathrm{BD},d}}\right)}{\partial\overline{\delta q}} & \frac{\partial\left(\overline{\dot{\hat{\omega}}^{\mathrm{B}}_{\mathrm{BD},d}}\right)}{\partial\overline{\delta\mathrm{B}}} & \frac{\partial\left(\overline{\dot{\hat{\omega}}^{\mathrm{B}}_{\mathrm{BD},d}}\right)}{\partial\omega^{\mathrm{B}}_{\mathrm{BD}}} & \frac{\partial\left(\overline{\dot{\hat{\omega}}^{\mathrm{B}}_{\mathrm{BD},d}}\right)}{\partial\bar{\hat{\rho}}^{\mathrm{B}}} & \frac{\partial\left(\overline{\dot{\hat{\omega}}^{\mathrm{B}}_{\mathrm{BD},d}}\right)}{\partial\bar{p}_{\mathrm{B}}} \end{bmatrix}\right|_{\tilde{\hat{q}}_{\mathrm{BD}},\tilde{\hat{\omega}}^{\mathrm{B}}_{\mathrm{BD}},\tilde{\bar{p}}_{\mathrm{B}}} \tag{34}$$

which, using the $\dot{\hat{\omega}}^{\mathrm{B}}_{\mathrm{BD}}$ expression from Eq. (16), results in:

$$\mathrm{F}_{\mathrm{dyn}}(t) = \begin{bmatrix} \frac{\partial\left(\overline{\dot{\hat{\omega}}^{\mathrm{B}}_{\mathrm{BD},r}}\right)}{\partial\overline{\delta q}} & 0_{3\times3} & \frac{\partial\left(\overline{\dot{\hat{\omega}}^{\mathrm{B}}_{\mathrm{BD},r}}\right)}{\partial\omega^{\mathrm{B}}_{\mathrm{BD}}} & 0_{3\times3} & \frac{\partial\left(\overline{\dot{\hat{\omega}}^{\mathrm{B}}_{\mathrm{BD},r}}\right)}{\partial\bar{p}_{\mathrm{B}}} \\ 0_{3\times3} & 0_{3\times3} & \left[-\overline{\tilde{\hat{\rho}}}^{\times}\right] & -2\left[\overline{\tilde{\omega}^{\mathrm{B}}_{\mathrm{DI}}}^{\times}\right] & 0_{3\times3} \end{bmatrix} \tag{35}$$

with

In Eq. (36), $\bar{u}_{\mathrm{B}} = \left[\frac{I_{xx}}{I_{yy}}, \frac{I_{zz}}{I_{yy}}, \frac{I_{xx}}{I_{zz}}\right]^{\mathrm{T}}$ and the 3×3 matrix quantities $\mathrm{M}_a(\cdot,\cdot)$, $\mathrm{M}_b(\cdot,\cdot)$, $\mathrm{M}_{aa}(\cdot,\cdot)$, $\mathrm{N}_p(\cdot)$, $\mathrm{F2}_p(\cdot,\cdot,\cdot)$, and $\mathrm{F3}_p(\cdot,\cdot,\cdot)$ as well as the derivation of Eqs. 35,36 are pro-

$$\begin{aligned}\frac{\partial\left(\dot{\overline{\tilde{\omega}}}^{\mathrm{B}}_{\mathrm{BD},r}\right)}{\partial\overline{\delta q}} &= 2\left\{\mathrm{M}_b\left(\overline{\tilde{\omega}}^{\mathrm{B}}_{\mathrm{BD}},\tilde{\tilde{u}}_{\mathrm{B}}\right)+\mathrm{M}_a\left(\overline{\tilde{\omega}}^{\mathrm{B}}_{\mathrm{BD}},\tilde{\tilde{u}}_{\mathrm{B}}\right)+\mathrm{M}_{aa}\left(\tilde{\tilde{p}}_{\mathrm{B}},\overline{\tilde{\omega}}^{\mathrm{B}}_{\mathrm{DI}}\right)+\left[\overline{\tilde{\omega}}^{\mathrm{B}}_{\mathrm{BD}}{}^{\times}\right]\right\}\left[\overline{\tilde{\omega}}^{\mathrm{B}}_{\mathrm{DI}}{}^{\times}\right]-2\left[\overline{\tilde{\omega}}^{\mathrm{B}}_{\mathrm{DI}}{}^{\times}\right]\\ \frac{\partial\left(\dot{\overline{\tilde{\omega}}}^{\mathrm{B}}_{\mathrm{BD},r}\right)}{\partial\overline{\omega}^{\mathrm{B}}_{\mathrm{BD}}} &= \mathrm{M}_{aa}\left(\tilde{\tilde{p}}_{\mathrm{B}},\overline{\tilde{\omega}}^{\mathrm{B}}_{\mathrm{BD}}\right)+\mathrm{M}_a\left(\overline{\tilde{\omega}}^{\mathrm{B}}_{\mathrm{DI}},\tilde{\tilde{u}}_{\mathrm{B}}\right)+\mathrm{M}_b\left(\overline{\tilde{\omega}}^{\mathrm{B}}_{\mathrm{DI}},\tilde{\tilde{u}}_{\mathrm{B}}\right)-\left[\overline{\tilde{\omega}}^{\mathrm{B}}_{\mathrm{DI}}{}^{\times}\right]\\ \frac{\partial\left(\dot{\overline{\tilde{\omega}}}^{\mathrm{B}}_{\mathrm{BD},r}\right)}{\partial\overline{\tilde{p}}_{\mathrm{B}}} &= \mathrm{N}_p\left(\overline{\tilde{\omega}}^{\mathrm{B}}_{\mathrm{BD}}\right)+\mathrm{F2}_p\left(\overline{\tilde{\omega}}^{\mathrm{B}}_{\mathrm{BD}},\overline{\tilde{\omega}}^{\mathrm{B}}_{\mathrm{DI}},\tilde{\tilde{p}}_{\mathrm{B}}\right)+\mathrm{F3}_p\left(\overline{\tilde{\omega}}^{\mathrm{B}}_{\mathrm{BD}},\overline{\tilde{\omega}}^{\mathrm{B}}_{\mathrm{DI}},\tilde{\tilde{p}}_{\mathrm{B}}\right)+\mathrm{N}_p\left(\overline{\tilde{\omega}}^{\mathrm{B}}_{\mathrm{DI}}\right)\end{aligned}. \tag{36}$$

vided in the Appendix Section A. The assembly of $\mathrm{F}_{\mathrm{kin}}(t)$ and $\mathrm{F}_{\mathrm{dyn}}(t)$ into $\mathrm{F}_{n\times n}(t)$ is provided later in Section 4.

3.2.3. Predictor step

The predictor step of the filter performs state and covariance time update. Accordingly, between the generic time instances t_{k^+} and $t_{(k+1)^-}$, the full state as defined in Eq. (21) is propagated as:

$$\tilde{\xi}_{(k+1)^-}=\tilde{\xi}_{k^+}+\int_{t_{k^+}}^{t_{(k+1)^-}} f(\xi(t),0,t)dt \tag{37}$$

where $\tilde{\xi}_k$ is the estimated full state at time t_k and one-step of the fifth-order DOPRI5 integrator of Dormand and Prince (1980) is employed. After each integration step, the unit dual quaternion structure is re-imposed through (Filipe et al., 2015):

$$\begin{aligned}\left[q_{\mathrm{BD},r}\right] &= \frac{\left[q_{\mathrm{BD},r}\right]}{\left\|\left[q_{\mathrm{BD},r}\right]\right\|}\\ \left[q_{\mathrm{BD},d}\right] &= \left(\mathrm{I}_4-\frac{\left[q_{\mathrm{BD},r}\right]\left[q_{\mathrm{BD},r}\right]^{\mathrm{T}}}{\left\|\left[q_{\mathrm{BD},r}\right]\right\|^2}\right)\left[q_{\mathrm{BD},d}\right].\end{aligned} \tag{38}$$

The covariance is propagated linearly. Given the typical time steps used in noncooperative pose estimation problems (corresponding to measurements update rates of 1 Hz or faster), the following approximation for the state transition matrix Φ can be adopted:

$$\Phi(\Delta t)=\mathrm{I}_n+\mathrm{F}_{n\times n}(t_{k^+})\Delta t \tag{39}$$

where $\Delta t=t_{(k+1)^-}-t_{k^+}$ and $\mathrm{F}_{n\times n}$ is defined in Eq. (30). By denoting $\Phi(\Delta t)=\Phi_{k,k+1}$, the propagation of the covariance matrix is performed as (Montenbruck and Gill, 2001):

$$\mathrm{P}_{n\times n}\left(t_{(k+1)^-}\right)=\Phi_{k,k+1}\,\mathrm{P}_{n\times n}(t_{k^+})\,\Phi_{k,k+1}^{\mathrm{T}}+\mathrm{Q}_{n\times n}\left(t_{(k+1)^-}\right) \tag{40}$$

where $\mathrm{Q}_{n\times n}(t)$ is the contribution of the process noise computed through:

$$\mathrm{Q}_{n\times n}\left(t_{(k+1)^-}\right)=\mathrm{C}_{n\times n}^{\mathrm{T}}\left(t_{(k+1)^-}\right)\mathrm{D}_{n\times n}\left(t_{(k+1)^-}\right) \tag{41}$$

with

$$\begin{bmatrix}\mathrm{C}_{n\times n}\\ \mathrm{D}_{n\times n}\end{bmatrix}\left(t_{(k+1)^-}\right)=e^{\left(\breve{\mathrm{F}}_{2n\times 2n}\left(t_{k^+}\right)\Delta t\right)}\begin{bmatrix}0_{n\times n}\\ \mathrm{I}_{n\times n}\end{bmatrix} \tag{42}$$

and

$$\breve{\mathrm{F}}_{2n\times 2n}(t_{k^+})=\begin{bmatrix}-\mathrm{F}_{n\times n}(t_{k^+}) & \mathrm{G}_{n\times p}(t_{k^+})\Sigma_{p\times p}\mathrm{G}_{n\times p}^{\mathrm{T}}(t_{k^+})\\ 0_{n\times n} & \mathrm{F}_{n\times n}^{\mathrm{T}}(t_{k^+})\end{bmatrix}. \tag{43}$$

As for the propagation of the process noise, the approach of Hou et al. (2017) is used, though swapping $\mathrm{F}_{n\times n}(t_{k^+})$ and $-\mathrm{F}_{n\times n}(t_{k^+})$ in the diagonal of $\breve{\mathrm{F}}_{2n\times 2n}$ (see Eq. (43))) to obtain $\mathrm{C}_{n\times n}^{\mathrm{T}}\mathrm{D}_{n\times n}$ instead of $\mathrm{C}_{n\times n}\mathrm{D}_{n\times n}^{-1}$ in Eq. (41).

3.2.4. Corrector step

In the corrector step, both state and covariance matrix are updated based on the information brought by a new observation. At the filter level, the measurement obtained from the sensing device or from its specific data processing unit can be modeled as the noisy attitude and noisy relative distance between a point Q on the target and the chaser reference frame {D} (*i.e.*, position and mounting direction of the sensor on the chaser are known or calibrated accurately):

$$q_{\mathrm{QD},m}\qquad \bar{r}^{\mathrm{D}}_{\mathrm{QD},m}. \tag{44}$$

Accordingly, depending on the architecture of the navigation system, Q may be a feature detected on the target (denoted by P_i), hence related to the pixel coordinates on an image through the perspective-n-points equations (Pasqualetto Cassinis et al., 2021), or the origin of the geometric frame (G) as extracted by a 3D point cloud, or directly the center of mass B, if some knowledge on the mass distribution of the target is available to support the pre-processing algorithms. The pose of Q w.r.t. {D} is computed with Eq. (3) and it is related to the target-chaser relative pose $\hat{q}_{\mathrm{BD}}$ through:

$$\hat{q}_{\mathrm{QD}}=\hat{q}_{\mathrm{BD}}\hat{q}_{\mathrm{QB}}. \tag{45}$$

In our formulation, the term $\hat{q}_{\mathrm{QB}}$ is a constant parameter of the target, which by referring to the general structures of full and EKF states of Eqs. (21) and (23), is contained in s. The dual error quaternion associated with $\hat{q}_{\mathrm{QB}}$ is defined as:

$$\delta\hat{q}_{\mathrm{QB}}=\hat{q}_{\mathrm{QB}}\tilde{\hat{q}}^{*}_{\mathrm{QB}}. \tag{46}$$

By denoting with t_k the generic instant of time at which a new observation is provided, the measurement equations of the filter are written as:

$$z_m(t_k) = h_m(x(t_k)) + v_m(t_k) \in \mathbb{R}^m \tag{47}$$

where z_m and h_m are respectively the actual and the modeled observations; v_m is the measurement noise assumed to be a discrete Gaussian white noise contribution, with zero mean and covariance $\mathrm{R}_{m\times m} = \mathrm{E}\left[v_m v_m^{\mathrm{T}}\right] = \sigma_v^2 \mathrm{I}_m$.The measures' sensitivity matrix is defined as:

$$\mathrm{H}_{m\times n}(t_k) \triangleq \left.\frac{\partial h_n(x_n(t))}{\partial x_n}\right|_{\tilde{x}_n(t_{k^-})} \in \mathbb{R}^{m\times n} \tag{48}$$

and is evaluated at the estimated state immediately before the new observation. For the quaternion MEKF the most convenient way to present quaternion measurements is in terms of the adopted 3-dimensional parametrization to express the deviation between the observed and estimated attitudes (Markley, 2003). Extending this principle to the dual quaternion MEKF, the measurement equation to a single point of reference Q is written as:

$$z_6(t_k) = \overline{\tilde{\hat{q}}_{\mathrm{QB}}(t_{k^-}) \left(\tilde{\hat{q}}^*_{\mathrm{QD}}(t_{k^-})\, \hat{q}_{\mathrm{QD},m}(t_k)\right) \tilde{\hat{q}}^*_{\mathrm{QB}}(t_{k^-})} \in \mathbb{R}^6 \tag{49}$$

which conveys the deviation between observed and estimated poses of Q w.r.t. {D}, expressed in {B}. This latter rotation has been introduced to simplify the expression of the measurement equation as function of the filter state x_n, which is then given by:

$$h_6(t_k) = \overline{\delta\hat{q}_{\mathrm{BD}}(t_k)\, \delta\hat{q}_{\mathrm{QB}}}(t_k)\,. \tag{50}$$

Accordingly, $H_{m\times n}$ is only composed of the identity matrix blocks that convey the sensitivity w.r.t. $\overline{\delta\hat{q}_{\mathrm{BD}}}$ and $\overline{\delta\hat{q}_{\mathrm{QB}}}$. Again, within the first-order approximation, the magnitude of the scalar parts of the error quaternion components tends to 1. Note that the general expression of Eq. (49) covers all the cases of system state encompassed in Fig. 2, depending on the role assumed by Q. In the simplest form, when B is directly sensed, it simplifies to Eq. (45) of Filipe et al. (2015). In the case that the observations are provided to the filter as measured quaternion and relative displacement separately, the methodology just explained applies to the quaternion observation, whereas for the distance the vector measurement model approach of Markley (2003) is to be employed, as detailed in Gaias and Lovera (2022). At this point, the optimal Kalman state update is computed as:

$$\Delta^\star \tilde{x}_n(t_k) \triangleq \begin{bmatrix} \Delta^\star \overline{\tilde{\delta q}_{\mathrm{BD}}}(t_k) \\ \Delta^\star \overline{\tilde{\omega}^{\mathrm{B}}_{\mathrm{BD}}}(t_k) \\ \Delta^\star \tilde{s}^{\mathrm{B}}(t_k) \end{bmatrix} = \mathrm{K}_{n\times m}(t_k)\, z_6(t_k) \tag{51}$$

where $\mathrm{K}_{n\times m}(t_k)$ is the Kalman gain given by (Montenbruck and Gill, 2001):

$$\begin{aligned} &\mathrm{K}_{n\times m}(t_k) = \mathrm{P}_{n\times n}(t_{k^-})\, \mathrm{H}^{\mathrm{T}}_{m\times n}(t_k) \\ &\left[\mathrm{H}_{m\times n}(t_k)\, \mathrm{P}_{n\times n}(t_{k^-})\, \mathrm{H}^{\mathrm{T}}_{m\times n}(t_k) + \mathrm{R}_{m\times m}(t_k)\right]^{-1}. \end{aligned} \tag{52}$$

The covariance update is performed using the numerically more stable formulation provided in (Montenbruck and Gill, 2001):

$$\begin{aligned} \mathrm{P}_{n\times n}(t_{k^+}) = \; & [\mathrm{I}_n - \mathrm{K}_{n\times m}(t_k)\mathrm{H}_{m\times n}(t_k)]\mathrm{P}_{n\times n}(t_{k^-}) \\ & [\mathrm{I}_n - \mathrm{K}_{n\times m}(t_k)\mathrm{H}_{m\times n}(t_k)]^{\mathrm{T}} + \\ & + \mathrm{K}_{n\times m}(t_k)\mathrm{R}_{m\times m}(t_k)\mathrm{K}^{\mathrm{T}}_{n\times m}(t_k). \end{aligned} \tag{53}$$

where P_{k^-} is the state covariance right before t_k and $\mathrm{R}_{m\times m}$ is the covariance of the measurement noise.

3.2.5. Reset

The state update operation for a standard EKF is accomplished by $\tilde{x}_n(t_{k^+}) = \tilde{x}_n(t_{k^-}) + \Delta^\star \tilde{x}_n(t_k)$. In the MEKF framework, instead, a reset operation must be explicitly carried out in order to set to zero the postupdate value of $\overline{\delta q}(t_{k^+})$ prior to the time update step (Markley, 2003). As for the dual quaternion MEKF, first the scalar components of real and dual parts of $\Delta^\star \delta\tilde{\hat{q}}$ are reconstructed from $\Delta^\star \overline{\delta\tilde{\hat{q}}}$ using Eq. (50) of Filipe et al. (2015). For the sake of completeness, it is here recalled the expression assumed when the attitude error is smaller than 180 deg:

$$\begin{aligned} \Delta^\star \delta\tilde{\hat{q}} = \; & \left(\sqrt{1 - \left\|\Delta^\star \overline{\delta\tilde{\hat{q}}_r}\right\|^2}, \Delta^\star \overline{\delta\tilde{\hat{q}}_r}\right) + \\ & + \epsilon \left(-\frac{\Delta^\star \overline{\delta\tilde{\hat{q}}_r}^{\mathrm{T}}\, \Delta^\star \overline{\delta\tilde{\hat{q}}_d}}{\sqrt{1 - \left\|\Delta^\star \overline{\delta\tilde{\hat{q}}_r}\right\|^2}}, \Delta^\star \overline{\delta\tilde{\hat{q}}_d}\right) \end{aligned} \tag{54}$$

which makes use of Eqs. (1) and (4). Afterwards, the pose components of the state are updated in compliance to the definition of the dual error quaternion (*i.e.*, reported in Eqs. (22) and (46) for the states considered in this work). Ad example, for the target-chaser relative pose it becomes:

$$\tilde{\hat{q}}_{\mathrm{BD}}(t_{k^+}) = \tilde{\hat{q}}_{\mathrm{BD}}(t_{k^-})\, \Delta^\star \tilde{\hat{q}}_{\mathrm{BD}}(t_k)\,. \tag{55}$$

4. Multiplicative extended Kalman filters for 6 DoF relative state and parameters estimation

This section shows how the general structure of the dual quaternion MEKF described in Section 3.2 specifies to address a set of particular cases, covering the needs of both loosely- and tightly-coupled architectures of the close-range navigation system.

4.1. Kinematic MEKF for state estimation

The first case is the simplest realization of the dual quaternion MEKF to achieve a kinematic estimation of the relative 6-DoF state only. This option suits a loosely-coupled architecture approach, where the sensor data processing unit is able to provide (pseudo) measurements of the principal axis frame {B} directly. Hence, with reference to Eq. (44), Q is actually B, and the filter aims at refining the input measurements while reconstructing the full 6-DoF relative state. Essentially this realization is the dual quaternion MEKF of Filipe et al. (2015) in the special case with no angular or linear velocity measurements (note that the component $\hat{b}$ of Filipe et al. (2015) is $-\hat{\omega}^{\mathrm{B}}_{\mathrm{BD}}$). In this

work, the covariance is propagated linearly instead of integrating numerically the Riccati equation, to reduce the computational effort while achieving comparable performance. In this specific case, the full state of the system is the $\xi^{(1)}$ of Fig. 2, and all the design variables of the filter become:

$$\begin{aligned} x_{12}^{(1)}(t) &= \left[\overline{\delta\hat{q}_{\mathrm{BD}}}^{\mathrm{T}} \quad \overline{\hat{\omega}_{\mathrm{BD}}^{\mathrm{B}}}^{\mathrm{T}}\right]^{\mathrm{T}} \\ w_6^{(1)}(t) &= \left[\bar{\epsilon}_{\omega}^{\mathrm{T}} \quad \bar{\epsilon}_{v}^{\mathrm{T}}\right]^{\mathrm{T}} \\ \mathrm{F}_{12\times12}^{(1)}(t) &= \begin{bmatrix} \mathrm{F}_{\mathrm{kin},6\times12}(t) \\ 0_{6\times12} \end{bmatrix} \\ \mathrm{G}_{12\times6}^{(1)} &= \begin{bmatrix} 0_{6\times6} \\ \mathrm{I}_6 \end{bmatrix} \\ \mathrm{H}_{6\times12}^{(1)} &= \begin{bmatrix} \mathrm{I}_6 & 0_{6\times6} \end{bmatrix} \\ \breve{\mathrm{H}}_{6\times12}^{(1)}(t) &= \begin{bmatrix} \mathrm{I}_3 & 0_{3\times3} & 0_{3\times3} & 0_{3\times3} \\ 0_{3\times3} & 2\tilde{\mathrm{R}}(t) & 0_{3\times3} & 0_{3\times3} \end{bmatrix}. \end{aligned} \tag{56}$$

where $\mathrm{H}_{6\times12}^{(1)}$ is the measure sensitivity matrix when the observations are provided in dual quaternion form (*i.e.*, $\hat{q}_{\mathrm{BD},m}$), $\breve{\mathrm{H}}_{6\times12}^{(1)}$ is the measure sensitivity matrix when relative attitude and distance observations are provided separately (*i.e.*, $q_{\mathrm{BD},m}$ and $\bar{r}_{\mathrm{BD},m}^{\mathrm{D}}$), and $\tilde{\mathrm{R}}(t) = \mathrm{R}\left(\tilde{\hat{q}}_{\mathrm{BD},r}^{*}(t)\right)$ denotes the rotation matrix associated with the conjugate of the estimated quaternion. From the structure of $\mathrm{F}_{12\times12}^{(1)}$ it can be noted that the relative angular and linear velocities are modeled as constants (up to the effect of process noise). Accordingly, their time varying behavior has to be caught by the process noise components $\bar{\epsilon}_{\omega}(t)$ and $\bar{\epsilon}_{v}(t)$. This implies that the tuning of the filter varies depending on the rotational motion of the target satellite (in the close-range region the domain of the relative linear velocities is limited to comply with relative trajectories suitable for close-range navigation over extended periods of time).

4.1.1. Propagation of measurement noise

The measurements of Eq. (44) can be modeled as the *true* quaternions affected by some 3D vector component errors:

$$\begin{aligned} q_m &= \frac{q+\epsilon_q}{\|q+\epsilon_q\|} \quad \text{with} \quad q = (q_0, \bar{q}) \quad \epsilon_q = \left(0, \bar{\epsilon}_q\right) \\ r_m &= r + \epsilon_r \quad \text{with} \quad r = (0, \bar{r}) \quad \epsilon_r = (0, \bar{\epsilon}_r) \end{aligned}. \tag{57}$$

Accordingly, both the normalization to obtain a unit quaternion and the construction of the unit dual quaternion through Eq. (3) are nonlinear functions of the error components $\bar{\epsilon}_q$ and $\bar{\epsilon}_r$. Following the approach of Aghili and Parsa (2009), here the propagation of the measurement errors is modeled, to formulate a state-dependent measurement covariance matrix (SDR) able to convey the first-order error propagation effects on the filter measurement equation of Eq. (47).

To this end, the measured quaternion is approximated as (Aghili and Parsa, 2009):

$$q_m \approx q + \left(\mathrm{I}_4 - qq^{\mathrm{T}}\right)\epsilon_q. \tag{58}$$

and the quaternion part of the measurement equation of Eq. (49) (related to the real part of $\tilde{\hat{q}}^{*}\hat{q}_m$) is given by:

$$\begin{aligned} z_{q,3}(t_k) &= \overline{\left[\tilde{\hat{q}}^{*}\hat{q}_m\right]_r} = \overline{\delta q}(t_k) + \bar{v}_{q,3}(t_k) \\ &\approx \overline{\delta q}(t_k) + \overline{\tilde{q}^{*}(t_k)\epsilon_q(t_k)} \end{aligned} \tag{59}$$

where $\bar{\cdot}$ is used to extract the vector part from a quaternion. The term $\overline{\tilde{q}^{*}(t_k)\epsilon_q(t_k)}$ can be written as $\mathrm{T}(t_k)\bar{\epsilon}_q(t_k)$ with

$$\mathrm{T}(t_k) = \tilde{q}_0\mathrm{I}_3 - [\bar{\tilde{q}}^{\times}] \in \mathbb{R}^{3\times3}. \tag{60}$$

As a result, the quaternion block of the SDR matrix is computed as:

$$\mathrm{R}_{q,3\times3}(t_k) = \mathrm{E}\left[\bar{v}_{q,3}(t_k)\bar{v}_{q,3}^{\mathrm{T}}(t_k)\right] = \mathrm{T}(t_k)\,\sigma_q^2\mathrm{I}_3\,\mathrm{T}^{\mathrm{T}}(t_k) \tag{61}$$

where σ_q is the standard deviation of the error quantity $\bar{\epsilon}_q$.

The measurement equation associated to the dual part of $\tilde{\hat{q}}^{*}\hat{q}_m$ is given by:

$$\begin{aligned} z_{d,3}(t_k) = \overline{\left[\tilde{\hat{q}}^{*}\hat{q}_m\right]_d} &= \overline{\delta\mathrm{B}}(t_k) + \bar{v}_{d,3}(t_k) \\ &\approx \overline{\delta\mathrm{B}}(t_k) + \breve{\mathrm{T}}(t_k)\begin{bmatrix} \bar{\epsilon}_q(t_k) \\ \bar{\epsilon}_r(t_k) \end{bmatrix} \end{aligned} \tag{62}$$

where the short-hand notation introduced in Section 3.2.2 is used for $\delta\mathrm{B}$. The quantity $\breve{\mathrm{T}}(t_k)$ is computed by carrying out the dual quaternion operations and retaining only the first-order contributions, to obtain:

$$\breve{\mathrm{T}}(t_k) = \begin{bmatrix} -\tilde{q}_0\mathrm{I}_3\left[\bar{\tilde{r}}^{\times}\right] & \frac{1}{2}\mathrm{I}_3 \end{bmatrix} \in \mathbb{R}^{3\times6} \tag{63}$$

where the approximations $\delta q_0 \approx 1$ and $\overline{\delta q} \approx \bar{0}$ have been also employed. Then the block of the SDR matrix associated with the dual part of the measurement equation becomes:

$$\begin{aligned} \mathrm{R}_{d,3\times3}(t_k) &= \mathrm{E}\left[\bar{v}_{d,3}(t_k)\bar{v}_{d,3}^{\mathrm{T}}(t_k)\right] \\ &= \breve{\mathrm{T}}(t_k)\,\mathrm{diag}\left(\sigma_q^2\mathrm{I}_3, \sigma_r^2\mathrm{I}_3\right)\breve{\mathrm{T}}^{\mathrm{T}}(t_k) \end{aligned} \tag{64}$$

where σ_r is the standard deviation of the error quantity $\bar{\epsilon}_r$. The overall SDR matrix is structured as:

$$\mathrm{R}_{,6\times6}(t_k) = \mathrm{diag}(\mathrm{R}_{r,3\times3}(t_k), \mathrm{R}_{d,3\times3}(t_k)). \tag{65}$$

4.2. Dynamic MEKF for state and inertia ratios estimation

This second realization of the filter is the dynamical enhancement of the previous case, in the attempt to improve the estimation accuracy of the dual velocity component as well as to enable the estimation of the target inertia ratios' vector. The so-obtained filtering scheme is suitable for a loosely-coupled navigation system, where again the sensor data processing unit is able to provide (pseudo) measurements of the principal axis frame {B} directly (*i.e.*, Q = B) while the filter allows refining the knowledge of the target mass inertia properties. In this

case, the full state of the system is $\xi^{(2)}$ of Fig. 2, and all the design quantities of the filter become:

$$\begin{aligned} x_{15}^{(2)}(t) &= \left[\overline{\delta\hat{q}_{\mathrm{BD}}}^{\mathrm{T}} \quad \overline{\hat{\omega}_{\mathrm{BD}}^{\mathrm{B}}}^{\mathrm{T}} \quad \bar{p}_{\mathrm{B}}^{\mathrm{T}}\right]^{\mathrm{T}} \\ w_{6}^{(2)}(t) &= \left[\bar{\epsilon}_{\tau}^{\mathrm{T}} \quad \bar{\epsilon}_{f}^{\mathrm{T}}\right]^{\mathrm{T}} \\ \mathrm{F}_{15\times15}^{(2)}(t) &= \begin{bmatrix} \mathrm{F}_{\mathrm{kin},6\times12}(t) & 0_{6\times3} \\ \mathrm{F}_{\mathrm{dyn},6\times15}(t) & \\ 0_{3\times15} & \end{bmatrix} \\ \mathrm{G}_{15\times6}^{(2)}(t) &= \begin{bmatrix} 0_{6\times6} \\ \mathrm{Z}_{6\times6}(t) \\ 0_{3\times6} \end{bmatrix} \\ \mathrm{H}_{6\times15}^{(2)} &= \left[\mathrm{H}_{6\times12}^{(1)} \quad 0_{6\times3}\right] \\ \breve{\mathrm{H}}_{6\times15}^{(2)}(t) &= \left[\breve{\mathrm{H}}_{6\times12}^{(1)}(t) \quad 0_{6\times3}\right] \end{aligned} \tag{66}$$

with

$$\begin{aligned} \mathrm{Z}_{6\times6}(t) &= \begin{bmatrix} \mathrm{J}_{3\times3}(\bar{p}_{\mathrm{B}}) & 0_{3\times3} \\ 0_{3\times3} & \mathrm{I}_{3} \end{bmatrix} \\ \mathrm{J}_{3\times3}(\bar{p}_{\mathrm{B}}) &= \mathrm{diag}\left(1, \frac{1-p_y}{1+p_x}, \frac{1+p_z}{1-p_x}\right). \end{aligned} \tag{67}$$

The main differences w.r.t. Eq (56) are: the structure of $\mathrm{F}_{15\times15}$ is now based on the Jacobian of the dual quaternion relative dynamics equations (as derived in Section 3.2.2), the process noise components now represent unmodeled relative disturbance angular and linear accelerations, and with reference to $\mathrm{G}_{15\times6}$, the effect of the process noise on the rotational dynamics is now function of $\bar{p}_{\mathrm{B}}$ with the functional expression of $\mathrm{J}_{3\times3}(\bar{p}_{\mathrm{B}})$. Note that, since the rotational relative dynamics equations are written as $\dot{\omega}_{\mathrm{BI}}^{\mathrm{B}} - \dot{\omega}_{\mathrm{DI}}^{\mathrm{B}}$, the relative process noise component can be expressed as:

$$\bar{\epsilon}_{\tau_{\mathrm{BD}}} = \mathrm{J}_{3\times3}(\bar{p}_{\mathrm{B}})\bar{\epsilon}_{\tau_{\mathrm{B}}} - \tilde{\mathrm{R}}\mathrm{J}_{3\times3}(\bar{p}_{\mathrm{D}})\bar{\epsilon}_{\tau_{\mathrm{D}}}. \tag{68}$$

where the torque perturbation for each body i is defined as (see Aghili and Parsa (2009)):

$$\bar{\epsilon}_{\tau_i} = \left[\frac{\tau_x}{I_{xx}}, \frac{\tau_y}{I_{xx}}, \frac{\tau_z}{I_{xx}}\right]^{\mathrm{T}}. \tag{69}$$

Hence, Eq (67) states that the unmodeled torque disturbances on the chaser can be neglected, since the disturbances affecting the known chaser satellite can be modeled very precisely. Numerical evidence shows that this approach allows a faster convergence to the true value of $\bar{p}_{\mathrm{B}}$ w.r.t. employing $\mathrm{I}_{3\times3}\bar{\epsilon}_{\tau_{\mathrm{BD}}}$, as performed in Gaias and Lovera (2022). The component $\bar{\epsilon}_f$ represents the relative disturbance accelerations, which in ADR scenarios are mainly composed of the differential J_2 and aerodynamic drag contributions; both are small indeed in the close-range region thanks to cancellation effects.

4.3. Dynamic MEKF for state and parameters estimation

This section describes a dynamic MEKF to estimate the inertia ratios of the target and the position and orientation of the target principal axes frame. Accordingly, this is the extension of the basic dynamic MEKF to retrieve the full set of estimable target parameters. As depicted in Fig. 2, this realization can support both loosely- and tightly-coupled approaches. In the first case, the filter receives the noisy pose measurements of the geometric frame {G} w.r.t. {D} (*i.e.*, in Eq. (44) Q = G). This is a very realistic approach, since pose determination algorithms - either processing LiDAR or visual images data - generally rely on wireframe models of the target satellite (Opromolla et al., 2017; Pasqualetto Cassinis et al., 2019). However, the estimation of the $\hat{q}_{\mathrm{GB}}$ pose becomes mandatory to achieve a 6-DoF solution that can be propagated in time to obtain an accurate prediction as required by certain close proximity operations. In a tightly-coupled approach, instead, the observations are measures of a Point of Reference (PoR) on the target, which represents a detected feature (Q = P). This case is here mentioned to introduce the tightly-coupled perspective, since in reality more than one feature is required to unambiguously resolve the pose of an object (Fischer and Bolles, 1981).

In both cases, for this realization the full state of the system is $\xi^{(3)}$ of Fig. 2 (*i.e.*, P = G), and all the design quantities of the filter become:

$$\begin{aligned} x_{21}^{(3)}(t) &= \left[\overline{\delta\hat{q}_{\mathrm{BD}}}^{\mathrm{T}} \quad \overline{\hat{\omega}_{\mathrm{BD}}^{\mathrm{B}}}^{\mathrm{T}} \quad \bar{p}_{\mathrm{B}}^{\mathrm{T}} \quad \overline{\delta\hat{q}_{\mathrm{GB}}}^{\mathrm{T}}\right]^{\mathrm{T}} \\ w_{12}^{(3)}(t) &= \left[w_{6}^{(2)} \quad \epsilon_{6,c}^{\mathrm{T}}\right]^{\mathrm{T}} \\ \mathrm{F}_{21\times21}^{(3)}(t) &= \begin{bmatrix} \mathrm{F}_{15\times15}^{(2)}(t) & 0_{15\times6} \\ 0_{6\times15} & 0_{6\times6} \end{bmatrix} \\ \mathrm{G}_{21\times12}^{(3)}(t) &= \begin{bmatrix} \mathrm{G}_{15\times6}^{(2)}(t) & 0_{15\times6} \\ 0_{6\times6} & \mathrm{I}_{6} \end{bmatrix} \\ \mathrm{H}_{6\times21}^{(3)} &= \left[\mathrm{H}_{6\times15}^{(2)} \quad \mathrm{I}_{6}\right] \\ \breve{\mathrm{H}}_{6\times21}^{(3)}(t) &= \left[\mathrm{T}_{\mathrm{G},3\times3}(t) \quad 0_{6\times9} \quad \mathrm{C}_{\mathrm{G},3\times3}(t)\right] \end{aligned} \tag{70}$$

with

$$\begin{aligned} \mathrm{T}_{i,3\times3}(t) &= \begin{bmatrix} \mathrm{I}_{3} & 0_{3\times3} \\ -2\tilde{\mathrm{R}}\left[\overline{\tilde{r}_{i\mathrm{B}}^{\mathrm{B}}}^{\times}\right] & 2\tilde{\mathrm{R}} \end{bmatrix} \\ \mathrm{C}_{i,3\times3}(t) &= \begin{bmatrix} \mathrm{I}_{3} & 0_{3\times3} \\ -4\tilde{\mathrm{R}}\left[\overline{\tilde{r}_{i\mathrm{B}}^{\mathrm{B}}\tilde{q}_{i\mathrm{B}}^{*}}^{\times}\right] & 2\tilde{\mathrm{R}} \end{bmatrix}. \end{aligned} \tag{71}$$

The main differences w.r.t. Eq (66) are: the inclusion of a fictitious process noise contribution $\epsilon_{6,c}^{\mathrm{T}}$ to support the estimation of the 6 components of $\overline{\delta\hat{q}_{\mathrm{GB}}}$ and the structure of the measurement sensitivity matrices. As expressed in Eq (50), in fact, the measurement equation is now function of both $\overline{\delta\hat{q}_{\mathrm{BD}}}$ and $\overline{\delta\hat{q}_{\mathrm{GB}}}$. The main difference between this realization and the filter developed by the Authors in Gaias and Lovera (2022) is that the pose of {G} w.r.t. {B} is here expressed in dual quaternion, hence obtaining a fully consistent dual quaternion-based filtering scheme.

A further difference is the definition of $G_{21\times12}$, as already recalled in Section 4.2.

4.4. Dynamic MEKF for state and parameters estimation using multiple detected features

This last case addresses the dynamic MEKF that suites a tightly-coupled approach for simultaneous estimation of the relative 6-DoF state and target's parameters. For the sake of explanation, in this realization three features are detected on the target, denoted by the P_i points, $i = 1, 2, 3$. Accordingly, the full state of the system is $\xi^{(4)}$ of Fig. 2: all the arbitrary frames associated with each detected feature P_i are oriented as the geometric reference frame ($q_{P_iB} = q_{GB}$) and the 3D vectors $\bar{r}_{P_jB}$ (with $j = 2, 3$) become part of the filter state. The remaining design quantities become:

$$
\begin{aligned}
x_{27}^{(4)}(t) &= \left[\overline{\delta\hat{q}_{BD}}^{T} \;\; \overline{\hat{\omega}_{BD}^{B}}^{T} \;\; \bar{p}_{B}^{T} \;\; \overline{\delta\hat{q}_{P_1B}}^{T} \;\; \bar{r}_{P_2B}{}^{T} \;\; \bar{r}_{P_3B}{}^{T}\right]^{T} \\
w_{18}^{(3)}(t) &= \left[w_{12}^{(3)} \;\; \epsilon_{6,P}^{T}\right]^{T} \\
F_{27\times27}^{(4)}(t) &= \begin{bmatrix} F_{21\times21}^{(3)}(t) & 0_{21\times6} \\ 0_{6\times21} & 0_{6\times6} \end{bmatrix} \\
G_{27\times18}^{(3)}(t) &= \begin{bmatrix} G_{21\times12}^{(3)}(t) & 0_{21\times6} \\ 0_{6\times12} & I_6 \end{bmatrix} \\
\breve{H}_{6\times27}^{(4)}(t) &= \begin{bmatrix} T_{P_1,3\times3} & 0_{6\times9} & C_{P_1,3\times3} & 0_{6\times6} \\ T_{P_2,3\times3} & 0_{6\times9} & \begin{matrix} I_3 & 0_{3\times3} \\ 0_{3\times3} & 0_{3\times3} \end{matrix} & \begin{matrix} 0_{3\times3} & 0_{3\times3} \\ \tilde{R} & 0_{3\times3} \end{matrix} \\ T_{P_3,3\times3} & 0_{6\times9} & \begin{matrix} I_3 & 0_{3\times3} \\ 0_{3\times3} & 0_{3\times3} \end{matrix} & \begin{matrix} 0_{3\times3} & 0_{3\times3} \\ 0_{3\times3} & \tilde{R} \end{matrix} \end{bmatrix}
\end{aligned}
\tag{72}
$$

With respect to Eq (70), a further fictitious process noise contribution $\epsilon_{6,P}^{T}$ in included to support the estimation of the 3-j components of $\bar{r}_{P_jB}$. As for the measure sensitivity matrix, only the formulation where quaternion and distances are provided separately is reported. In tightly-coupled approaches, in fact, this matrix has to be pre-multiplied by the one that conveys how the specific design-related observations relate to such quaternion and distances. For example, if the navigation system relies on image processing, then observations are the 2D pixel coordinates of each P_i on the image and the perspective-n-points equations are used to compute the partials of the observation w.r.t. quaternion and distance to P_i (see for instance the H_i^{int} terms of Pasqualetto Cassinis et al. (2021)).

5. Simulations and Results

The performance of the filters described in the previous section are evaluated into a MATLAB®/Simulink® simulation environment, which models the spacecraft 6 DoF dynamics subject to perturbations and the measurements from the electro-optical sensor.

To this end, a scenario representative of active debris removal missions in low Earth orbit is considered. Accordingly, the target satellite orbits into a Sun-synchronous almost-circular orbit at ≈775 km of height on the Earth surface, where the aerodynamic perturbation is too weak to enable a natural orbit decay. The target satellite is tumbling with angular rate of arbitrarily direction and magnitude of 10 degrees per second. The chaser spacecraft observes the target from an almost bounded, centered, passively safe relative orbit, where this latter aspect is guaranteed through parallel relative eccentricity/inclination vectors. This kind of relative trajectory is an operationally convenient option to support inspection phases during close proximity operations (Gaias and Lovera, 2021; Gaias and Lovera, 2020). As for the satellites, target and chaser are taken similar to the spacecraft of the Prototype Research Instruments and Space Mission Technology Advancement (PRISMA) mission (D'Amico et al., 2013). In particular, the target is similar to the Tango satellite with approximately $0.60 \times 0.80 \times 0.31$ meters size and principal moments of $I_{xx} = 2.61, I_{yy} = 1.61$, and $I_{zz} = 3.54$ kg m^2. Whereas the chaser is customized on the Mango satellite. Given the small size of the target object, the magnitudes of the relative eccentricity and relative inclination vectors are both taken equal to 4 meters. Hence the chaser has already successfully concluded the mid-range rendezvous and starts observing the target in the close-range region. During the relative motion, the chaser keeps the boresight of the electro-optical sensor - in this work mounted as the y axis of the reference system {D} - directed towards the target, to keep it in its field of view (Gaias and Ardaens, 2018). This operational requirement determines attitude and angular rate of the chaser satellite.

In the following simulations, rotational and translational displacements between {G} and {B} are respectively taken as $\bar{q}_{GB} = [0.026, -0.009, 0.017]^{T}$ (corresponding to a rotation of ≈ 3.7 degrees) and $\bar{r}_{GB}^{B} = [0.01, -0.02, 0.02]^{T}$ meters. Such numerical values emulate the discrepancy between the two body-fixed frames generated by the use in the sensor' processing unit of a wireframe model of the tiny target satellite with no detailed knowledge of the mass distribution.

The measurements are modeled through additive white Gaussian noise affecting the true values as in Eq. (57). The standard deviation of the noise on the vector part of the measured quaternion is equal to 0.012 (3σ), which corresponds to a rotation error of magnitude of ≈ 6 degrees. The standard deviation of the noise affecting the measure of relative separation is set equal to 0.015 meters (3σ). These parameters are inline with the values considered in similar studies published so far (*e.g.*, (Filipe et al., 2015; Aghili and Parsa, 2009; Hou et al., 2017)).

The initial guess of the filter is set to emulate the knowledge of the relative state at conclusion of the mid-range

rendezvous. In particular, the center of mass position and velocity of the target satellite are expected to be known with respectively decimeter and centimeter per second accuracy, as obtained by processing angles-only and range measurements. Based on the results of the AVANTI (Autonomous Vision Approach Navigation and Target Identification) angles-only far-range noncooperative rendezvous (Ardaens and Gaias, 2018b; Ardaens and Gaias, 2018a; Gaias and Ardaens, 2018), in fact, below 50 m of inter-satellite separation the direct measurement of the range is suggested to improve the accuracy and robustness of the relative navigation solution. The error on the knowledge of the target angular rate is taken of approximately 0.6 degrees per second to emulate the coarse estimation of debris angular rate from ground observations. To emulate a rendezvous to a partially known target satellite, the errors on the inertia ratios are taken as 20% of the maximum inertia ratio.

5.1. Kinematic MEKF

This section presents the performance of the kinematic MEKF. For the sake of comparison with the work of Filipe et al. (2015), the sensor provides pose measurements at 10 Hz. The tunable parameters of the filter are: the state covariance at initial time $\mathrm{P}_{12\times12}(0) = 10^{-4}\,\mathrm{I}_{12}$ (see Eq. (40)) and covariance matrix of the process noise $\Sigma = 10^{-4}\,\mathrm{I}_6$ (see Eq. (27)). Recall that in this formulation the tuning of the process noise depends on the values of relative angular and linear rates.

Two simulations are reported respectively to investigate the effect of employing a state-dependent measurements covariance matrix (see Fig. 3) and and to compare the behavior when the pseudo-measurements are provided directly as a dual quaternion pose or as quaternion and relative distance separately (see Fig. 4).

In all cases the kinematic filter refines well the input measurements (*i.e.*, yellow points in the left views) and estimates the full relative 6 DoF state with an accuracy in line with the previously published results (Filipe et al., 2015). The performance is measured in terms of magnitude of the estimation error, computed from the scalar part for the unit error quaternion $2\cos^{-1}(\delta q_0)$ and from the 2-norm of the vector part for vector error quaternions $\|\bar{q} - \tilde{\bar{q}}\|$. As for Fig. 3, it can be noted that the modeling of the first-order error propagation effects on the filter measurement equation through a SDR (blue) has a negligible impact w.r.t. the overall estimation accuracy (see results for constant R in black). Fig. 4 shows how the estimation accuracy is basically the same when the (pseudo) measurements are either provided directly in dual quaternion form (black) or as quaternion and relative distance separately (green). By combining the two aforementioned findings, when applicable, it is suggested to assemble the observations into a unit dual quaternion and to use a constant R. The former simplifies the structure of H (see Eqs. (56)–(70)); the latter simplifies the computation of the optimal state update (see Eqs. 52,53).

5.2. Comparison between dynamic and kinematic MEKF

This section presents the comparison between the kinematic filter (k-MEKF) and its dynamic counterpart (d-MEKF). To this end, the same scenario of Section 5.1 is employed. The tuning of the k-MEKF is the same of before, whereas for the dynamic MEKF it is set: $\mathrm{P}_{15\times15}(0) = \mathrm{diag}\left(10^{-4}\,\mathrm{I}_{12}, 10^{-1}\,\mathrm{I}_3\right)$ and $\Sigma = 10^{-6}\,\mathrm{I}_6$.

Fig. 5 compares the estimation errors in pose and dual velocity: as expected the dynamic filter improves the accuracy of the estimated solution, especially in the velocity components. This is extremely important in proximity

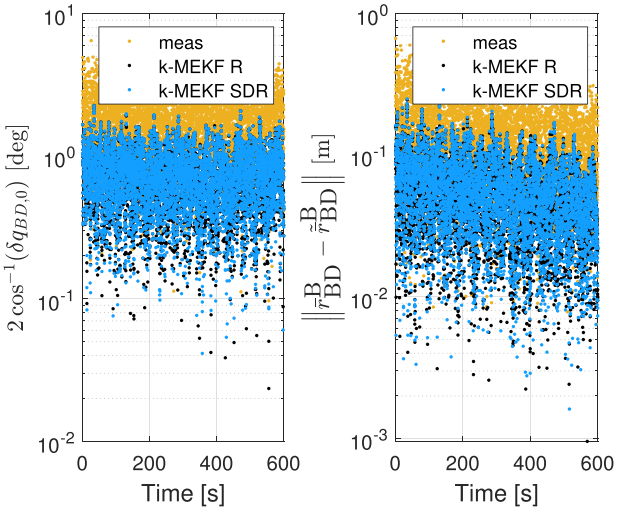

a) Magnitude of pose error.

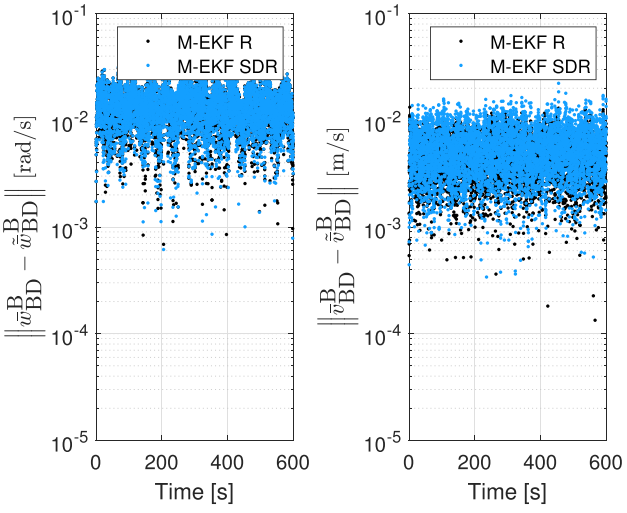

b) Magnitude of dual velocity error.

Fig. 3. Kinematic MEKF receiving pose measurements: constant vs state-dependent (SDR) measurement covariance matrix R.

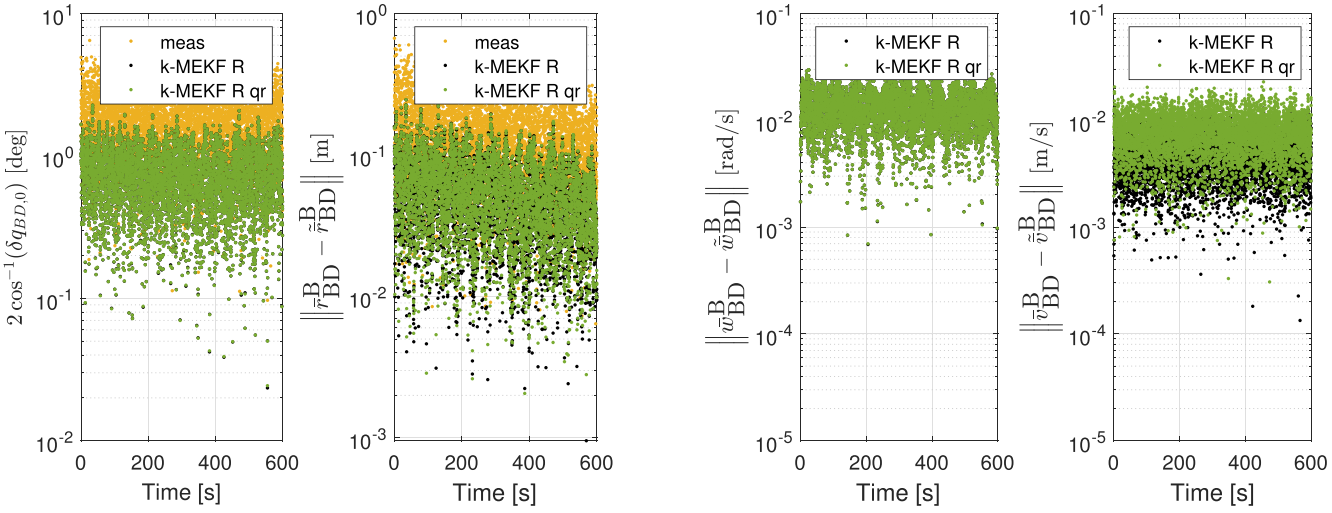

a) Magnitude of pose error. b) Magnitude of dual velocity error.

Fig. 4. Kinematic MEKF receiving either pose or quaternion and relative displacement (qr) measurements.

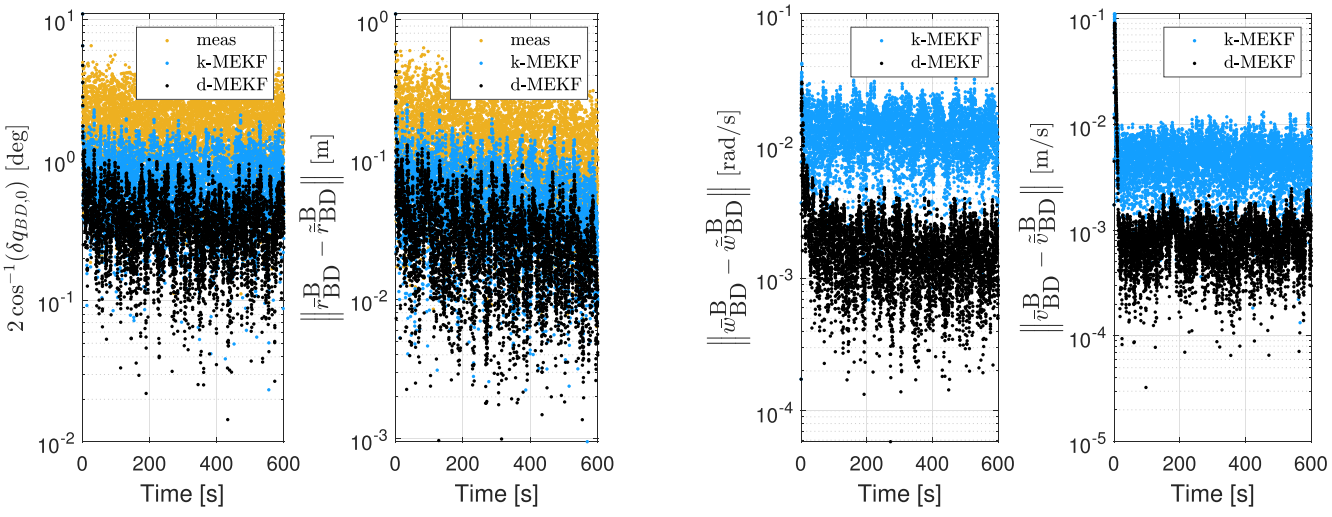

a) Magnitude of pose error. b) Magnitude of dual velocity error.

Fig. 5. Comparison between dynamic (d-, black) and kinematic-only (k-, blue) MEKF.

operations around noncooperative targets, to plan the relative attitude at future time and thus to better support guidance and capture tasks. Moreover, as depicted in the right view of Fig. 6, the errors in the knowledge of the inertia ratios is nullified in less than 100 s (black plots), making the relative attitude prediction more reliable. The left view of Fig. 6, instead, shows the achievable estimation accuracy in the dual velocity components (for the specific simulation case under consideration) when the dynamic filter is not estimating the $\bar{p}_B$ part of the state - in green - (*i.e.*, the initial values affected by a 20% error are kept unvaried throughout the simulation). This is the numerical evidence of the importance of estimating the main target's parameters together with the full relative state. As for the proposed filter structure, enabling the estimation of $\bar{p}_B$ is simply achieved by providing proper values to the initial covariance components associated to the inertia ratios. As a result, it has been shown that for loosely-coupled architectures in which only the 6 DoF relative state is reconstructed using a dynamic filtering scheme allows achieving a more accurate solution than what achievable by kinematic schemes. Moreover, the proposed filter can seamlessly enable the estimation/refinement of the target's inertia ratios, while keeping the original loosely-coupled architecture structure. This allows a further improvement of the estimated solution. Note that, if required to improve the overall robustness in the presence of very large errors in the initial conditions, an architecture employing sequential kinematic and dynamic MEKFs may be considered.

A last simulation is run, introducing the aforementioned small rotational and translational displacements between {G} and {B} to emulate the impact of limited knowledge

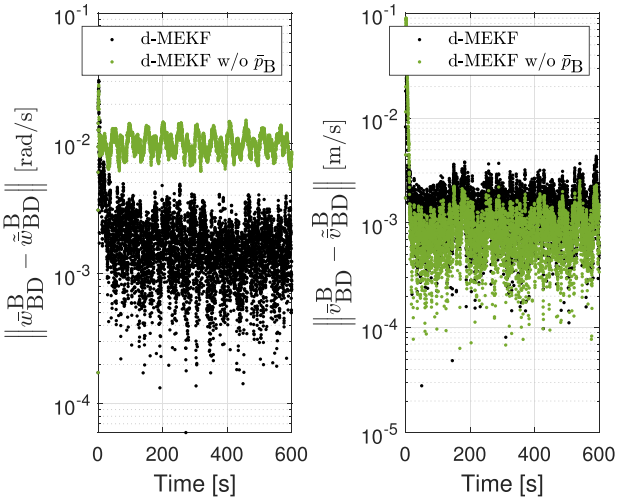

a) Magnitude of dual velocity error.

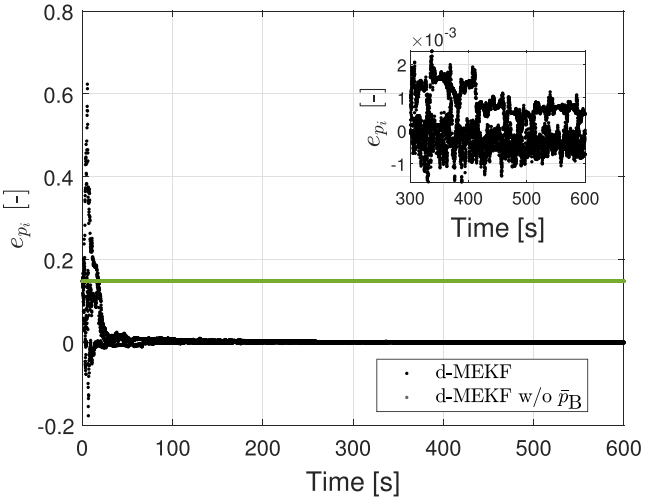

b) Estimation error of the p_i components.

Fig. 6. Dynamic MEKF with (black) and without (green) estimation of $\bar{p}$.

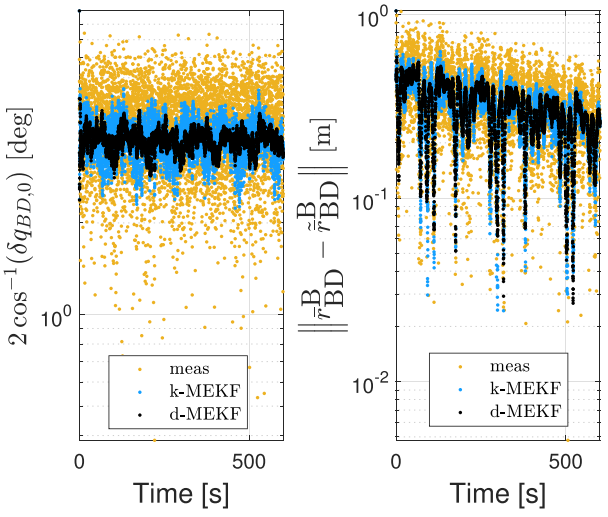

a) Magnitude of pose error.

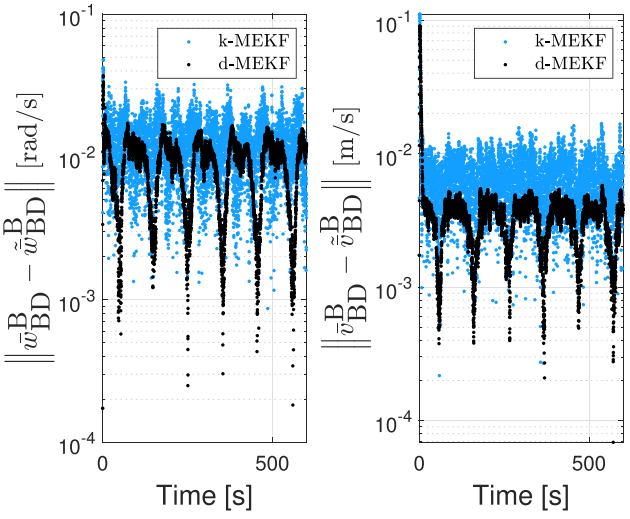

b) Magnitude of dual velocity error.

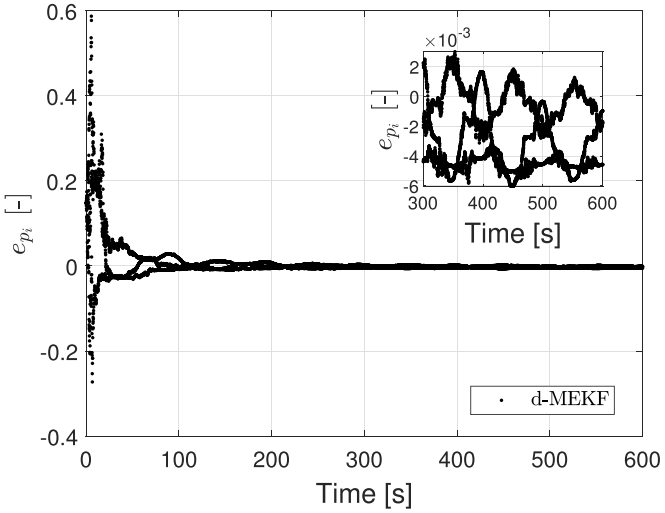

c) Estimation error of the p_i components.

Fig. 7. Dynamic estimation (state expressed in {B}), when the pose observations are $\hat{q}_{\mathrm{GD},m}$.

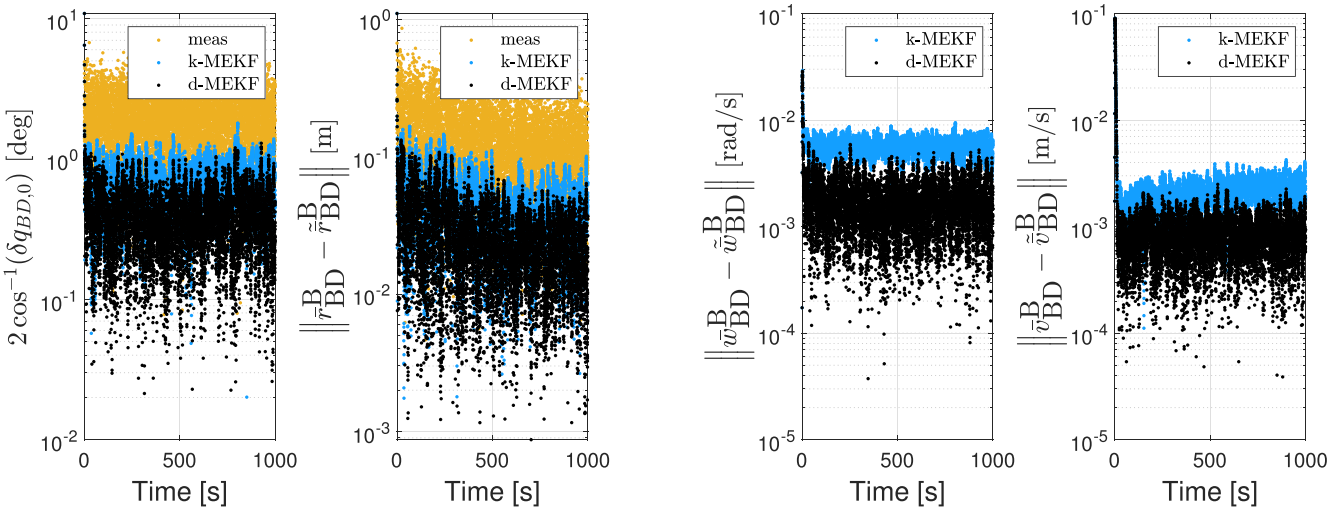

a) Magnitude of pose error.

b) Magnitude of dual velocity error.

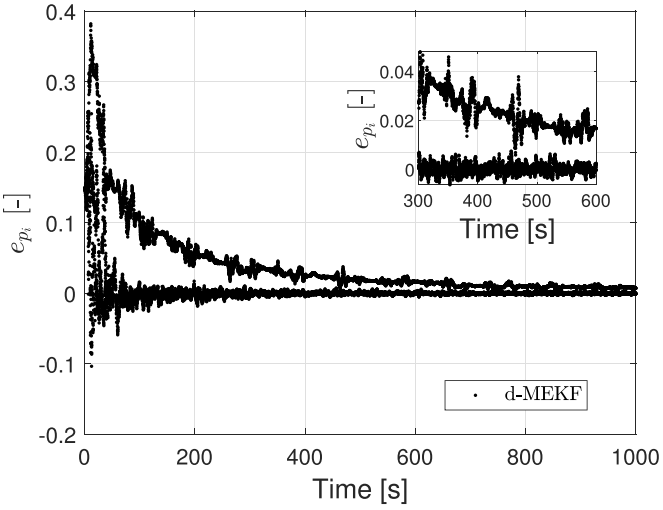

c) Estimation error of the p_i components.

Fig. 8. Slowly tumbling target: comparison between dynamic (d-, black) and kinematic-only (k-, blue) MEKF.

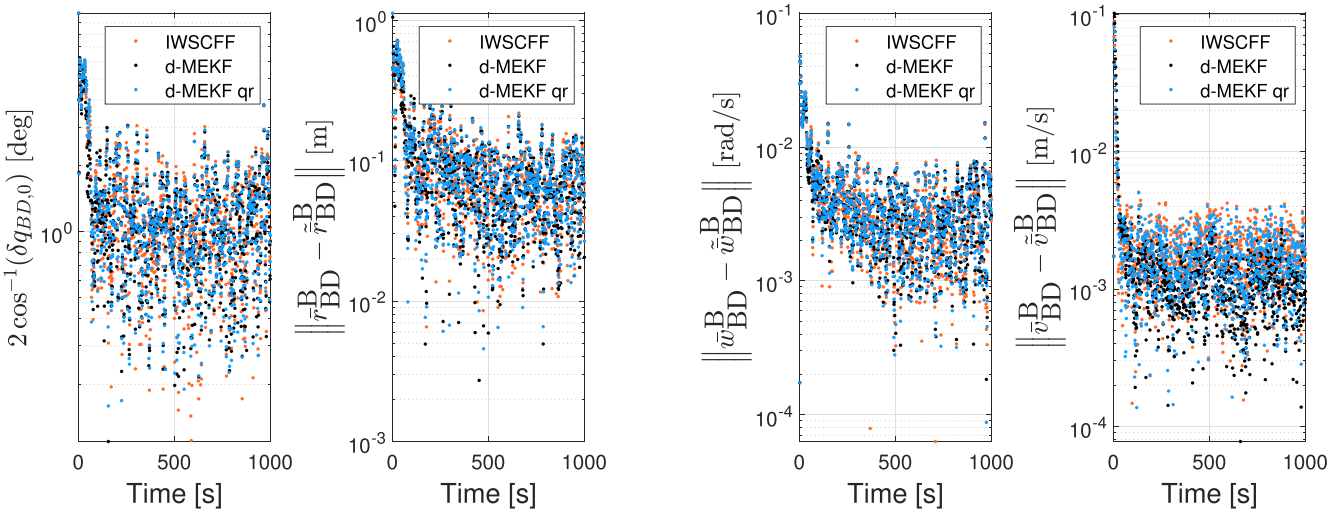

a) Magnitude of pose error.

b) Magnitude of dual velocity error.

Fig. 9. Dynamic MEKF for state and parameters estimation fed by either pose or quaternion and relative displacement (qr) measurements: 6 DoF relative state estimation.

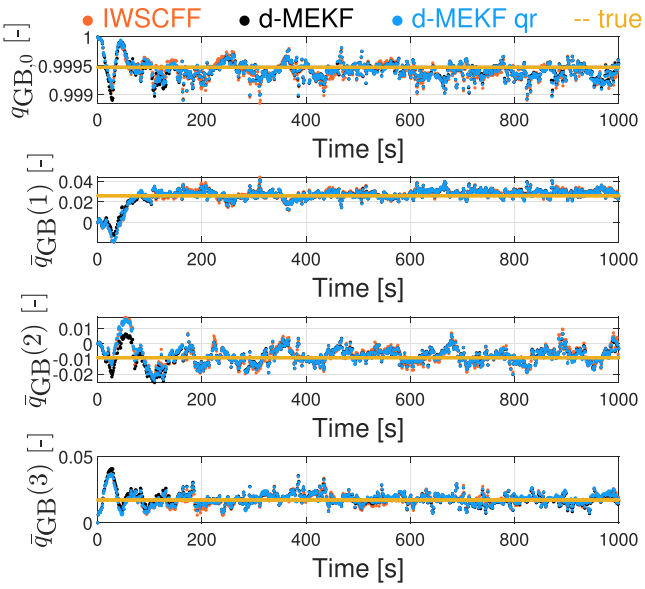

a) Orientation of {B}.

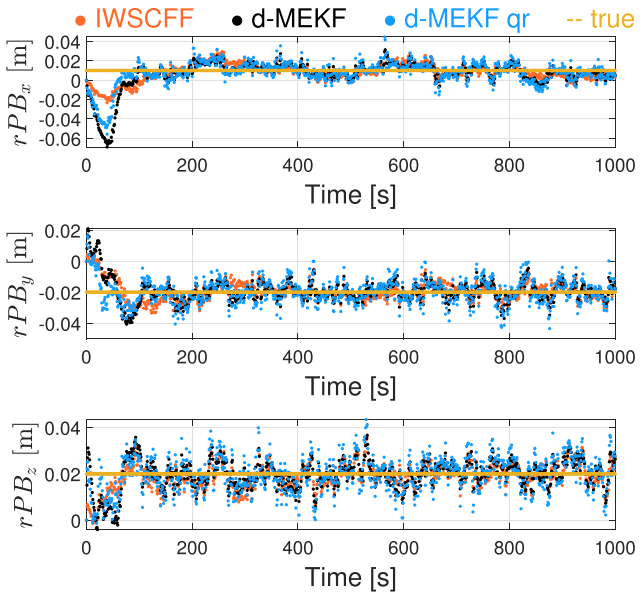

b) Position of the origin of {B}

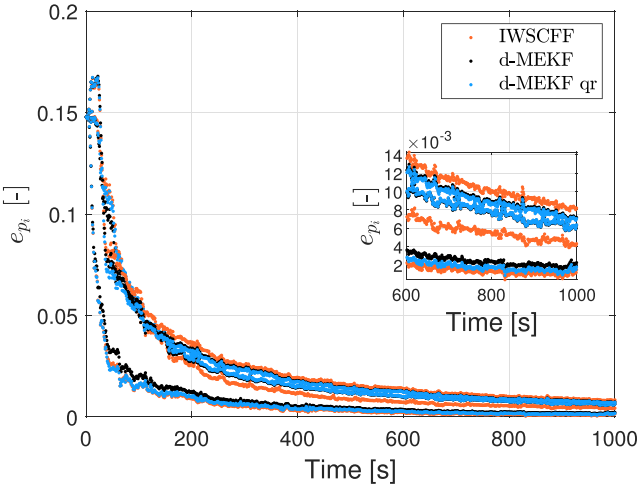

c) Estimation error of the p_i components.

Fig. 10. Dynamic MEKF for state and parameters estimation fed by either pose or quaternion and relative displacement (qr) measurements: parameters' estimation.

of the mass distribution of the target satellite. Accordingly, the pseudo measurements refer to the geometric reference system, as output of algorithms that make use of a simple wireframe model of the target satellite ($\hat{q}_{\mathrm{GD},m}$). The error metrics, instead, refer to the quantities expressed in the principal axes reference frame {B}, to measure the accuracy of the estimated solution w.r.t. the *true* dynamics of the target. Fig. 7 presents the obtained results in this case, comparing the performances of kinematic (in blue) and dynamic (in black) filters. Indeed there is still filtering capability of the measurement noise (observations are marked in yellow) and again the dynamic scheme outperforms the kinematic filter. Nonetheless, the estimated state is affected by an error that reflects the effective displacement between the reference systems. This is obvious in the rotational component of the magnitude of the pose error view. As for the accuracy of the estimation of the dual relative velocity, one can compare the views Fig. 7 b) and Fig. 5 b), where the observations were not affected by modeling error between {G} and {B}. This numerical assessment motivates the need to estimate position and orientation of the target principal axes frame - in addition to the inertia ratios, when the observations have been obtained referring on a geometric frame though an accurate solution is required.

5.2.1. Inertia ratios estimation for slowly tumbling targets

This subsection shows the behavior of the dynamic filter when the tiny target satellite tumbles at a slower rate than what considered so far. This analysis is performed to test

the filter into a more demanding condition for the estimation of the augmented state. In the specific, the magnitude of the absolute angular rate of the target is now set as ≈ 4 degrees per seconds; whereas all the other parameters of the simulation are kept as before. As for the tuning, the covariance matrix of the process noise for the kinematic filter is set equal to $\Sigma = 10^{-6}\mathrm{I}_6$. Fig. 8 collects the state and parameters estimation errors for this specific case, using the same color-code employed in Section 5.2. The inertia ratios are properly estimated despite the relatively slow angular rate of the target (see view Fig. 8 c)). As expected, more time is required to recover the initial error in the knowledge of the inertia ratios.

5.3. Dynamic MEKF for state and full-set parameters' estimation

This section presents the performance of the dynamic MEKF when state and the full set of parameters are estimated and the filter receives as (pseudo) measurements the pose to the geometric reference system of the target satellite $\hat{q}_{\mathrm{GD},m}$. Accordingly, this formulation of the filter addresses the limitations highlighted in Fig. 7. By referring to Eq. (70), this case is challenging since a state of dimension 21 is to be estimated from 6-dimensional observations. The same scenario employed so far is considered, though the measurement update rate is now set equal to 1 Hz, which is a typical feasible value for running the image processing algorithms on an onboard processor (Aghili and Parsa, 2009; Capuano et al., 2019; Pasqualetto Cassinis et al., 2021).

As for this simulation, the following tuning has been adopted: $\mathrm{P}_{21\times 21}(0) = \mathrm{diag}\left(10^{-4}\mathrm{I}_{12}, 10^{-3}\mathrm{I}_3, 10^{-8}\mathrm{I}_3\right)$ and $\Sigma = \mathrm{diag}\left(10^{-6}\mathrm{I}_6, 10^{-5}\mathrm{I}_6\right)$. Figs. 9 shows the estimation error for the state. Fig. 10 presents the error of estimation of the considered parameters, namely orientation of the principal axes frame a), position of the center of mass b), and ratios of the moments of inertia c). For the sake of generality, also the filter implemented by the Authors in Gaias and Lovera (2022) - here denoted by the label IWSCFF - has been considered. This latter, in fact, presents another possible implementation in the specific case where measures to a single point of reference are provided. As can be noted, there is no meaningful difference in terms of performance when the observations are provided in the form of a unit dual quaternion pose (black) or unit quaternion and relative displacement separately (blue). The relative 6 DoF state is estimated with the same accuracy of Fig. 5 (case in which the measurements were directly taken w.r.t. the {B} reference system). This proves the efficacy of the proposed formulation with augmented estimation state. In this case, in fact, the estimation of orientation and position of {B} is also achieved (see Fig. 10); the initial error has been set as if {G} were {B} (hence its magnitude reflects the true roto-translational displacement between the two considered reference frames). At the same time it is emphasized that, in the current - more challenging given the augmented size of the estimation state - case the simulation requires longer time to recover the initial error. Moreover, it is worth noting that the measurement update rate has been slowed down from 10 Hz for Fig. 5 (emulation of LiDAR) to 1 Hz for Fig. 10 (emulation of the output of a vision-based image processing). Based on the numerical investigations, the higher the target angular rate, the better the capability of the estimated solution to converge to true values. Nonetheless, thanks to the accurate motion modeling adopted in the filter development, convergence is obtained at a relatively low angular rate of the target. For the sake of comparison, the results shown in Aghili and Parsa (2009) for a similar scenario (*e.g.*, tiny almost symmetrical target spacecraft, comparable inter-

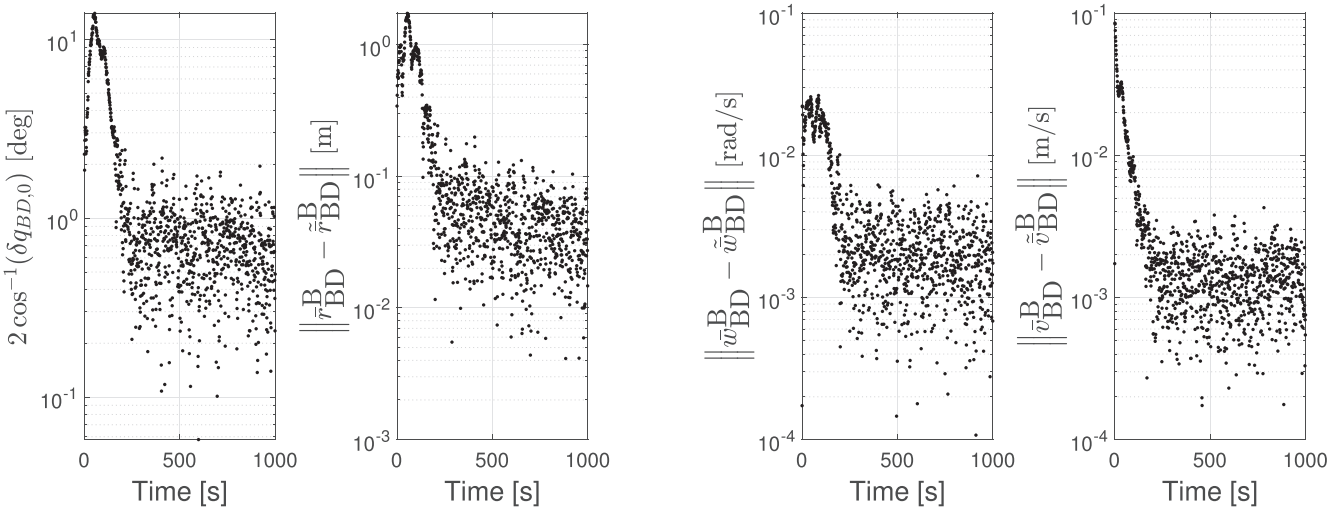

a) Magnitude of pose error. b) Magnitude of dual velocity error.

Fig. 11. Dynamic MEKF for tightly-coupled approaches fed by qr measurements of 3 detected features: 6 DoF relative state estimation.

satellite distance) have been obtained running the filter at 2 Hz and maximum component of the target angular rate of ≈ 28 deg/s.

5.4. Dynamic MEKF for state and full-set parameters' estimation using 3 detected features

This last section addresses the formulation to support tightly-coupled approaches and it is assumed that 3 features are detected on the target satellite. Scenario and measurement update rate are kept as in Section 5.3. By referring to Eqs. (72), due to the need to estimate the coordinates of the PoRs in $\{B\}$, the state becomes of dimension 27. Nonetheless, now at each measurement update step the observations' set is composed of the three poses of the measured PoRs. The detected features are selected as three vertexes of the target spacecraft.

As for this simulation, the following tuning has been adopted: $P_{27\times27}(0) = \mathrm{diag}\left(10^{-4}\mathrm{I}_{12}, 10^{-2}\mathrm{I}_3, 10^{-8}\mathrm{I}_3, 10^{-6}\mathrm{I}_6\right)$ and $\Sigma_0 = \mathrm{diag}\left(10^{-6}\mathrm{I}_6, 10^{-5}\mathrm{I}_6, 10^{-4}\mathrm{I}_6\right)$. The simulations results are collected in Fig. 11, in terms of full relative state, and Fig. 12, for the estimated parameters. Note that for this case the plots refer to the single realization of the filter provided in Eqs. (72). Referring to Fig. 11, one can note that the achievable accuracy is in line with the results obtained so far, though the transient to recover the initial

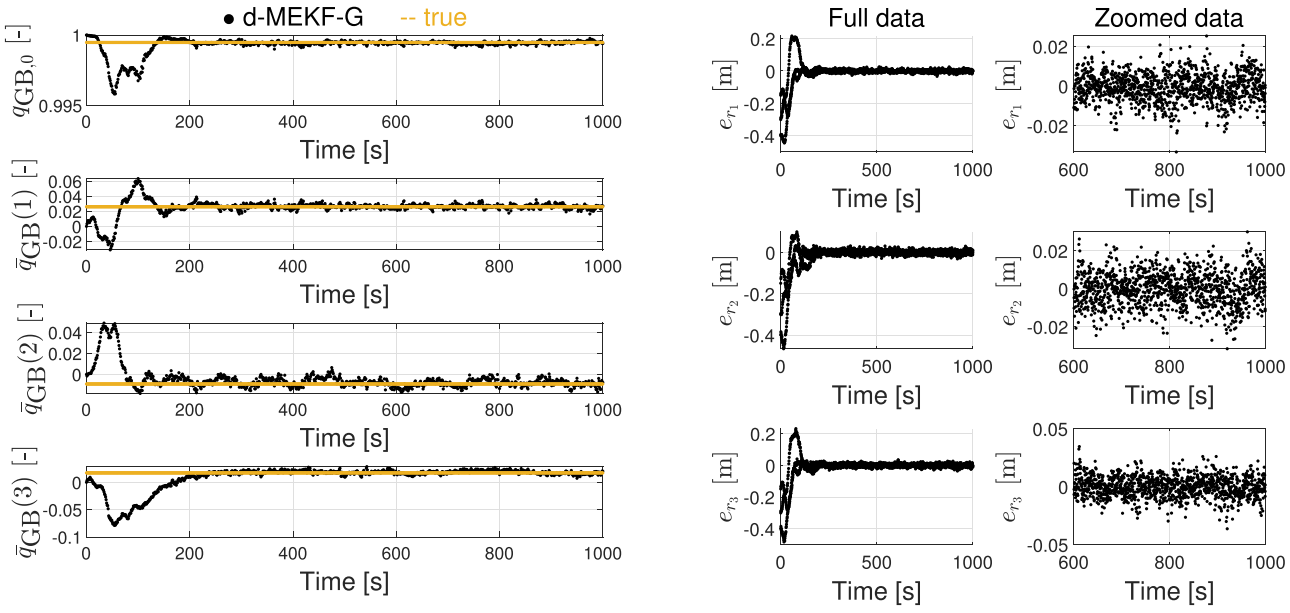

a) Orientation of {B}. b) Position errors of the 3 PoRs written in {B}

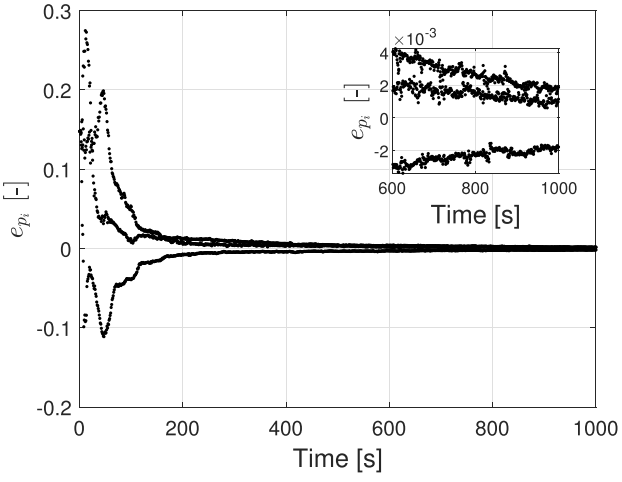

c) Estimation error of the p_i components.

Fig. 12. Dynamic MEKF for tightly-coupled approaches fed by qr measurements of 3 detected features: parameters' estimation.

error takes now a little bit more time (see for example Fig. 9). As for the estimation of the parameters (Fig. 12), the orientation of {B} a) and the ratios of the inertia moments c) are properly recovered in a shorter time with respect to the loosely-coupled architecture (Fig. 10). Indeed, in this case the filter benefits from receiving observations of multiple points of references. The b) plot of Fig. 12, specifically shows the 3 components estimation error for each of the three PoRs, which basically nullify after the first 200 s for the scenario under consideration.

6. Conclusion

This work addressed the need of estimating the relative roto-translational state and the main parameters of a non-cooperative target from an observing chaser satellite during close proximity operations. The design principle has been to attain a filter development that could serve different possible architectures of the close-range navigation system. This is motivated by the fact that indeed this kind of filtering activity is a common building block crosswise to the technical solutions proposed so far. Accordingly, a general approach is beneficial either to simplify the overall structure of the guidance, navigation and control system or to enhance its flexibility and adaptability to support the various phases of close proximity operations. Further design drivers have been the potential to extend this basic development to spaceborne implementations and/or to sensor fusion applications, which exploit a set of sensing devices, possibly operating at different rates.

In light of these motivations, this work developed a continuous-discrete, dual quaternion based, dynamic, multiplicative extended Kalman filter capable to deliver estimates of the full relative state, the ratios of the moments of inertia, and position and orientation of the principal frame of the target. No approximations on the relative six degrees-of-freedom motion have been introduced. And, for the sake of compactness, the equations of the relative roto-translational kinematics and dynamics have been represented in dual quaternions. To reflect the available technologies to observe in space a noncooperative target, the filter receives only pose measurements with respect to one or multiple arbitrary frames fixed on the target, depending whether a loosely- or tightly-coupled architecture is used for the navigation system. To demonstrate the generality of the proposed approach, different realizations have been presented, supported by an explanation of their possible utilization and numerical simulations to show their behavior within a scenario representative of the close-range inspection of a noncooperative target. Both measurement update rates of 10 and 1 Hz have been employed, to emulate the output of active laser and passive visual imaging respectively.

Results have shown that the current dynamic formulation outperforms previously published kinematic-only filters for pose estimation, both in terms of achievable accuracy and of enabling the estimation of the main target's parameters. Within the adopted dual quaternion formulation, it has been shown that (when applicable) it is convenient to provide the observations in terms of unit dual quaternion. This, in fact, allows reducing the measurement sensitivity matrix to a very simple form. At the same time, the propagation effect of the measurement errors through the nonlinear unit dual quaternion definition have a negligible impact on the achievable results. This allows employing anyway a constant covariance matrix of the measurement error.

Depending on the actual needs of the relative navigation system, the larger the size of the whole state to be estimated the more challenging the capability to recover the error on the initial guess. This is a structural characteristic of this problem, due to the technology limitations of obtaining only pose measurements from the observations. Out of the experience collected through numerical investigations it has been noted that, the faster the angular rate of the target the shorter the transient to estimate the values of the inertia ratios. Note that this aspect poses a conflicting requirement with respect to the data-processing algorithms either to extract features or to compute the target pose. Nonetheless, the obtained results have shown that when only the inertia ratios have to be estimated together with the relative state, this filter is capable to recover an error representative of the knowledge realistically available at the end of the mid-range rendezvous also for very low target's angular rate. Furthermore, when the full state is to be estimated, the current filter outperforms previously published results in the capability to converge with lower absolute angular rates of the target.

Declaration of competing interest

The authors declare that they have no known competing financial interests or personal relationships that could have appeared to influence the work reported in this paper.

Acknowledgments

The research leading to these results has received funding from the European Union's Horizon 2020 research and innovation programme under the Marie Skłodowska-Curie grant agreement No 793361 - ReMoVE (Rendezvous Modelling Visiting and Enhancing).

Appendix A. This section presents the derivation of Eqs. 35,36. To this end, the vector part of the real quaternion of the non-swapped Eq. (16) is written as:

$$\begin{aligned}\bar{\dot{\omega}}^{\mathrm{B}}_{\mathrm{BD},r} = \; & -\bar{\mathrm{I}}_{\mathrm{B}}^{-1}\left(\bar{\omega}^{\mathrm{B}}_{\mathrm{BD}} \times \left(\bar{\mathrm{I}}_{\mathrm{B}}\bar{\omega}^{\mathrm{B}}_{\mathrm{BD}}\right)\right) - \bar{\mathrm{I}}_{\mathrm{B}}^{-1}\left(\bar{\omega}^{\mathrm{B}}_{\mathrm{BD}} \times \left(\bar{\mathrm{I}}_{\mathrm{B}}\bar{\omega}^{\mathrm{B}}_{\mathrm{DI}}\right)\right) \\ & -\bar{\mathrm{I}}_{\mathrm{B}}^{-1}\left(\bar{\omega}^{\mathrm{B}}_{\mathrm{DI}} \times \left(\bar{\mathrm{I}}_{\mathrm{B}}\bar{\omega}^{\mathrm{B}}_{\mathrm{BD}}\right)\right) + \\ & -\bar{\mathrm{I}}_{\mathrm{B}}^{-1}\left(\bar{\omega}^{\mathrm{B}}_{\mathrm{DI}} \times \left(\bar{\mathrm{I}}_{\mathrm{B}}\bar{\omega}^{\mathrm{B}}_{\mathrm{DI}}\right)\right) - \left(\bar{\omega}^{\mathrm{B}}_{\mathrm{DI}} \times \bar{\omega}^{\mathrm{B}}_{\mathrm{BD}}\right) - \mathrm{R}_{\mathrm{D2B}}\bar{\dot{\omega}}^{\mathrm{D}}_{\mathrm{DI}} \\ = \; & f_1(\bar{\omega},\bar{p}) + f_2\left(\overline{\delta q},\bar{\omega},\bar{p}\right) + f_3\left(\overline{\delta q},\bar{\omega},\bar{p}\right) \\ & + f_4\left(\overline{\delta q},\bar{p}\right) + f_5\left(\overline{\delta q},\bar{\omega}\right) + f_6\left(\overline{\delta q}\right)\end{aligned} \tag{73}$$

where the f_1 to f_6 contributions have been highlighted together with the quantities on which they depend. Note that, for sake of conciseness, sub and superscripts have been dropped, hence: $\overline{\delta q} = \overline{\delta q}_{\mathrm{BD}}, \bar{\omega} = \bar{\omega}^{\mathrm{B}}_{\mathrm{BD}}$, and $\bar{p} = \bar{p}_{\mathrm{B}}$. The functional expressions of the partials of f_i w.r.t. the variables $\overline{\delta q}, \bar{\omega}$, and $\bar{p}$ are given by:

$$\begin{aligned} \frac{\partial f_1}{\partial \overline{\delta q}} &= \mathrm{M}_{aa}\left(\bar{p}_{\mathrm{B}}, \bar{\omega}^{\mathrm{B}}_{\mathrm{BD}}\right) \qquad \frac{\partial f_1}{\partial \bar{p}} = \mathrm{N}_p\left(\bar{\omega}^{\mathrm{B}}_{\mathrm{BD}}\right), \end{aligned} \tag{74}$$

$$\begin{aligned} \frac{\partial f_2}{\partial \overline{\delta q}} &= 2\mathrm{M}_b\left(\bar{\omega}^{\mathrm{B}}_{\mathrm{BD}}, \bar{u}_{\mathrm{B}}\right)\left[\tilde{\bar{\omega}}^{\mathrm{B}}_{\mathrm{DI}}{}^{\times}\right] \\ \frac{\partial f_2}{\partial \bar{\omega}} &= \mathrm{M}_a\left(\bar{\omega}^{\mathrm{B}}_{\mathrm{DI}}, \bar{u}_{\mathrm{B}}\right) \\ \frac{\partial f_2}{\partial \bar{p}} &= \mathrm{F2}_p\left(\bar{\omega}^{\mathrm{B}}_{\mathrm{BD}}, \bar{\omega}^{\mathrm{B}}_{\mathrm{DI}}, \bar{p}_{\mathrm{B}}\right), \end{aligned} \tag{75}$$

and

$$\begin{aligned} \frac{\partial f_3}{\partial \overline{\delta q}} &= 2\mathrm{M}_a\left(\bar{\omega}^{\mathrm{B}}_{\mathrm{BD}}, \bar{u}_{\mathrm{B}}\right)\left[\tilde{\bar{\omega}}^{\mathrm{B}}_{\mathrm{DI}}{}^{\times}\right] \\ \frac{\partial f_3}{\partial \bar{\omega}} &= \mathrm{M}_b\left(\bar{\omega}^{\mathrm{B}}_{\mathrm{DI}}, \bar{u}_{\mathrm{B}}\right) \\ \frac{\partial f_3}{\partial \bar{p}} &= \mathrm{F3}_p\left(\bar{\omega}^{\mathrm{B}}_{\mathrm{BD}}, \bar{\omega}^{\mathrm{B}}_{\mathrm{DI}}, \bar{p}_{\mathrm{B}}\right), \end{aligned} \tag{76}$$

where $\bar{u}_{\mathrm{B}} = \left[u_x, u_y, u_z\right]^{\mathrm{T}} = \left[\frac{I_{xx}}{I_{yy}}, \frac{I_{zz}}{I_{yy}}, \frac{I_{xx}}{I_{zz}}\right]^{\mathrm{T}}$ is a further representation of the ratios of the principal moments of inertia, and

$$\frac{\partial f_4}{\partial \overline{\delta q}} = 2\mathrm{M}_{aa}\left(\bar{p}_{\mathrm{B}}, \bar{\omega}^{\mathrm{B}}_{\mathrm{DI}}\right)\left[\tilde{\bar{\omega}}^{\mathrm{B}}_{\mathrm{DI}}{}^{\times}\right] \qquad \frac{\partial f_4}{\partial \bar{p}} = \mathrm{N}_p\left(\bar{\omega}^{\mathrm{B}}_{\mathrm{DI}}\right), \tag{77}$$

$$\frac{\partial f_5}{\partial \overline{\delta q}} = 2\left[\tilde{\bar{\omega}}^{\mathrm{B}}_{\mathrm{BD}}{}^{\times}\right]\left[\tilde{\bar{\omega}}^{\mathrm{B}}_{\mathrm{DI}}{}^{\times}\right] \qquad \frac{\partial f_5}{\partial \bar{\omega}} = -\left[\tilde{\bar{\omega}}^{\mathrm{B}}_{\mathrm{DI}}{}^{\times}\right], \tag{78}$$

$$\frac{\partial f_6}{\partial \overline{\delta q}} = -2\left[\tilde{\bar{\omega}}^{\mathrm{B}}_{\mathrm{DI}}{}^{\times}\right]. \tag{79}$$

The derivatives with respect to $\overline{\delta q}$ have been computed using:

$$\begin{aligned} \bar{v}^{\mathrm{B}} &= \mathrm{R}(q_{\mathrm{BD}})\bar{v}^{\mathrm{D}} = \mathrm{R}\left(\overline{\delta q}\right)\mathrm{R}(\tilde{q}_{\mathrm{BD}})\bar{v}^{\mathrm{D}} \\ &= \mathrm{R}\left(\overline{\delta q}\right)\tilde{\bar{v}}^{\mathrm{B}} \approx \left(\mathrm{I} - 2\left[\overline{\delta q}^{\times}\right]\right)\tilde{\bar{v}}^{\mathrm{B}} \end{aligned} \tag{80}$$

where $\mathrm{R}(\cdot)$ is the rotation matrix associated to the proper quaternion, so that:

$$\frac{\partial \bar{v}^{\mathrm{B}}}{\partial \overline{\delta q}} = 2\left[\tilde{\bar{v}}^{\mathrm{B}\times}\right]. \tag{81}$$

By introducing the notation $\bar{\omega} = \left[\omega_x, \omega_y, \omega_z\right]^{\mathrm{T}}$ for the general angular rate vector so that the associated vector quaternion is $\omega = (0, \bar{\omega})$ and $\bar{p} = \left[p_x, p_y, p_z\right]^{\mathrm{T}}$ for the vector of the inertia ratios as defined in Eq. (20), the matrix quantities appearing in (74)–(79) are given by:

$$\mathrm{M}_{aa}(\bar{p}, \bar{\omega}) = \begin{bmatrix} 0 & p_x\omega_x & p_x\omega_y \\ p_y\omega_z & 0 & p_y\omega_x \\ p_z\omega_y & p_z\omega_x & 0 \end{bmatrix}, \tag{82}$$

$$\mathrm{N}_p(\bar{\omega}) = \begin{bmatrix} \omega_y\omega_z & 0 & 0 \\ 0 & \omega_z\omega_x & 0 \\ 0 & 0 & \omega_x\omega_y \end{bmatrix}, \tag{83}$$

$$\mathrm{M}_a(\bar{\omega}, \bar{u}) = \begin{bmatrix} 0 & u_y\omega_z & -\omega_y/u_y \\ -\omega_z/u_z & 0 & u_z\omega_x \\ \omega_y/u_x & -u_x\omega_x & 0 \end{bmatrix}, \tag{84}$$

$$\mathrm{M}_b(\bar{\omega}, \bar{u}) = \begin{bmatrix} 0 & -u_x\omega_z & u_z\omega_y \\ \omega_z/u_x & 0 & -\omega_x/u_y \\ -\omega_y/u_z & u_y\omega_x & 0 \end{bmatrix}, \tag{85}$$

$$\mathrm{F2}_p(\bar{\omega}_1, \bar{\omega}_2, \bar{p}) = \begin{bmatrix} \frac{\omega_{1z}\omega_{2y}}{1-p_y} + \frac{\omega_{1y}\omega_{2z}}{1+p_z} & \frac{(1+p_x)\omega_{1z}\omega_{2y}}{(1-p_y)^2} & \frac{(1-p_x)\omega_{1y}\omega_{2z}}{(1+p_z)^2} \\ \frac{(1-p_y)\omega_{1z}\omega_{2x}}{(1+p_x)^2} & \frac{\omega_{1z}\omega_{2x}}{1+p_x} + \frac{\omega_{1x}\omega_{2z}}{1-p_z} & \frac{(1+p_y)\omega_{1x}\omega_{2z}}{(1-p_z)^2} \\ \frac{(1+p_z)\omega_{1y}\omega_{2x}}{(1-p_x)^2} & \frac{(1-p_z)\omega_{1x}\omega_{2y}}{(1+p_y)^2} & \frac{\omega_{1y}\omega_{2x}}{1-p_x} + \frac{\omega_{1x}\omega_{2y}}{1+p_y} \end{bmatrix}, \tag{86}$$

and

$$\mathrm{F3}_p(\bar{\omega}_1, \bar{\omega}_2, \bar{p}) = \begin{bmatrix} \frac{\omega_{1z}\omega_{2y}}{1+p_z} + \frac{\omega_{1y}\omega_{2z}}{1-p_y} & \frac{(1+p_x)\omega_{1y}\omega_{2z}}{(1-p_y)^2} & \frac{(1-p_x)\omega_{1z}\omega_{2y}}{(1+p_z)^2} \\ \frac{(1-p_y)\omega_{1x}\omega_{2z}}{(1+p_x)^2} & \frac{\omega_{1z}\omega_{2x}}{1-p_z} + \frac{\omega_{1x}\omega_{2z}}{1+p_x} & \frac{(1+p_y)\omega_{1z}\omega_{2x}}{(1-p_z)^2} \\ \frac{(1+p_z)\omega_{1x}\omega_{2y}}{(1-p_x)^2} & \frac{(1-p_z)\omega_{1y}\omega_{2x}}{(1+p_y)^2} & \frac{\omega_{1y}\omega_{2x}}{1+p_y} + \frac{\omega_{1x}\omega_{2y}}{1-p_x} \end{bmatrix}. \tag{87}$$

As a result, the partials of Eq. (36) are obtained as:

$$\begin{aligned} \frac{\partial\left(\overline{\dot{\bar{\omega}}^{\mathrm{B}}_{\mathrm{BD},r}}\right)}{\partial \overline{\delta q}} &= \frac{\partial f_2}{\partial \overline{\delta q}} + \frac{\partial f_3}{\partial \overline{\delta q}} + \frac{\partial f_4}{\partial \overline{\delta q}} + \frac{\partial f_5}{\partial \overline{\delta q}} + \frac{\partial f_6}{\partial \overline{\delta q}} \\ \frac{\partial\left(\overline{\dot{\bar{\omega}}^{\mathrm{B}}_{\mathrm{BD},r}}\right)}{\partial \bar{\omega}} &= \frac{\partial f_1}{\partial \bar{\omega}} + \frac{\partial f_2}{\partial \bar{\omega}} + \frac{\partial f_3}{\partial \bar{\omega}} + \frac{\partial f_5}{\partial \bar{\omega}} \\ \frac{\partial\left(\overline{\dot{\bar{\omega}}^{\mathrm{B}}_{\mathrm{BD},r}}\right)}{\partial \bar{p}} &= \frac{\partial f_1}{\partial \bar{p}} + \frac{\partial f_2}{\partial \bar{p}} + \frac{\partial f_3}{\partial \bar{p}} + \frac{\partial f_4}{\partial \bar{p}} \end{aligned} \tag{88}$$

to be evaluated at the estimated state.

References

Aghili, F., Parsa, K., 2009. Motion and parameter estimation of space objects using laser-vision data. J. Guidance Control Dyn. 32 (2), 538–550. https://doi.org/10.2514/1.37129.

Ardaens, J.-S., Gaias, G., 2018a. Angles-only relative orbit determination in low Earth orbit. Adv. Space Res. 31 (11), 2740–2760. https://doi.org/10.1016/j.asr.2018.03.016.

Ardaens, J.-S., Gaias, G., 2018b. Flight demonstration of spaceborne real-time angles-only navigation to a noncooperative target in low-Earth orbit. Acta Astronaut. 153, 367–382. https://doi.org/10.1016/j.actaastro.2018.01.044.

Benninghoff, H., Boge, T., 2015. Rendezvous involving a non-cooperative, tumbling target - estimation of moments of inertia and center of mass of an unknown target. In: Proceedings of the 25th International Symposium on Space Flight Dynamics ISSFD. DLR, German Space Operations Center, Munich, Germany.

Cao, L., Misra, A.K., 2015. Linearized J_2 and atmospheric drag model for satellite relative motion with small eccentricity. J. Aerospace Eng. 229 (14), 2718–2736. https://doi.org/10.1177/0954410015586843.

Capuano, V., Alimo, S.R., Ho, A.Q. et al., 2019. Robust features extraction for on-board monocular-based spacecraft pose acquisition. In: AIAA Scitech 2019 Forum. URL: https://arc.aiaa.org/doi/abs/10.2514/6.2019-2005. https://doi.org/10.2514/6.2019-2005. arXiv:https://arc.aiaa.org/doi/pdf/10.2514/6.2019-2005.

Crassidis, J.L., Markley, F.L., Cheng, Y., 2007. Survey of Nonlinear Attitude Estimation Methods. J. Guidance Control Dyn. 30 (1), 12–28. https://doi.org/10.2514/1.22452.

D'Amico, S., Ardaens, J.-S., Gaias, G., et al., 2013. Noncooperative rendezvous using angles-only optical navigation: system design and flight results. J. Guidance Control Dyn. 36 (6), 1576–1595. https://doi.org/10.2514/1.59236.

Dormand, J.R., Prince, P.J., 1980. A family of embedded Runge-Kutta formulae. J. Comput. Appl. Math. 6 (1), 19–26.

Filipe, N., Kontitsis, M., Tsiotras, P., 2015. Extended Kalman filter for spacecraft pose estimation using dual quaternions. J. Guidance Control Dyn. 38 (9), 1625–1641. https://doi.org/10.2514/1.G000977.

Filipe, N., Tsiotras, P., 2013a. Adaptive model-independent tracking of rigid body position and attitude motion with mass and inertia matrix identification using dual quaternions. AIAA Guidance, Navigation, and Control Conference, AIAA Paper 2013-5173 AIAA.

Filipe, N., Tsiotras, P., 2013b. Rigid body motion tracking without linear and angular velocity feedback using dual quaternions. In: European Control Conference Piscataway. IEEE Publ, NJ, pp. 329–334.

Filipe, N., Tsiotras, P., 2013c. Simultaneous position and attitude control without linear and angular velocity feedback using dual quaternions. Washington, DC: American Control Conference.

Filipe, N., Tsiotras, P., 2015. Adaptive position and attitude-tracking controller for satellite proximity operations using dual quaternions. J. Guidance Control Dyn. 38 (4), 566–577. https://doi.org/10.2514/1.G000054.

Fischer, M., Bolles, R., 1981. Random sample consensus: A paradigm for model fitting with applications to image analysis and automated cartography. Commun. ACM 24 (6), 381–395.

Gaias, G., Ardaens, J.-S., 2018. In-orbit experience and lessons learned from the AVANTI experiment. Acta Astronaut. 153, 383–393. https://doi.org/10.1016/j.actaastro.2018.01.042.

Gaias, G., Lovera, M., 2020. Safe trajectory design for close proximity operations. In: Advances in the Astronautical Sciences. Lake Tahoe, CA, USA: AAS/AIAA Astrodynamics Specialist Conference volume 175.

Gaias, G., Lovera, M., 2021. Trajectory design for proximity operations: the relative orbital elements' perspective. J. Guidance Control Dyn., Published Online:21 Sep 2021, https://doi.org/10.2514/1.G006175.

Gaias, G., Lovera, M., 2022. 6-DoF Relative State and Parameters Estimation for Close-Range Navigation to Noncooperative Targets. 22-50. Politecnico di Milano, Milan, Italy: 11th International Workshop on Satellite Constellations and Formation Flying.

Hou, X., Ma, C., Wang, Z., et al., 2017. Adaptive pose and inertial parameters estimation of free-floating tumbling space objects using dual vector quaternions. Adv. Mech. Eng. 9 (10), 1–17. https://doi.org/10.1177/1687814017714210.

Markley, F.L., 2003. Attitude error representations for Kalman filtering. J. Guidance Control Dyn. 26 (2), 311–317.

Montenbruck, O., Gill, E., 2001. Satellite Orbits - Models, Methods, and Applications. Springer Verlag.

Opromolla, R., Fasano, G., Rufino, G., et al., 2017. A review of cooperative and un-cooperative spacecraft pose determination techniques for close-proximity operations. Prog. Aerosp. Sci. 93, 53–72. https://doi.org/10.1016/j.paerosci.2017.07.001.

Pasqualetto Cassinis, L., Fonod, R., Gill, E., 2019. Review of the robustness and applicability of monocular pose estimation systems for relative navigation with an uncooperative spacecraft. Prog. Aerosp. Sci. 110, 100548. https://doi.org/10.1016/j.paerosci.2019.05.008.

Pasqualetto Cassinis, L., Fonod, R., Gill, E., et al., 2021. Evaluation of tightly- and loosely-coupled approaches in CNN-based pose estimation systems for uncooperative spacecraft. Acta Astronaut. 182, 189–202. https://doi.org/10.1016/j.actaastro.2021.01.035.

Pesce, V., Lavagna, M., Bevilacqua, R., 2017. Stereovision-based pose and inertia estimation of unknown and uncooperative space objects. Adv. Space Res. 59 (1), 236–251. https://doi.org/10.1016/j.asr.2016.10.002, URL: https://www.sciencedirect.com/science/article/pii/S0273117716305622.

Razgus, B., Mooij, E., Choukroun, D., 2017. Relative navigation in asteroid missions using dual quaternion filtering. J. Guidance Control Dyn. 40 (9), 2151–2166. https://doi.org/10.2514/1.G002805.

Segal, S., Gurfil, P., 2009. Effect of kinematic rotation-translation coupling on relative spacecraft translational dynamics. J. Guidance Control Dyn. 32 (3), 1045–1050. https://doi.org/10.2514/1.39320.

Sheinfeld, D., Rock, S.M., 2009. Rigid Body Inertia Estimation with Applications to the Capture of a Tumbling Satellite. 09-123. Savannah, Georgia,USA: 19th AAS/AIAA Space Flight Mechanics Meeting.

Wang, J., Sun, Z., 2012. 6-DOF robust adaptive terminal sliding mode control for spacecraft formation flying. Acta Astronaut. 73, 76–87. https://doi.org/10.1016/j.actaastro.2011.12.005.

Wang, X., Yu, C., 2010. Feedback linearization regulator with coupled attitude and translation dynamics based on unit dual quaternion. In: 2010 IEEE International Symposium on Intelligent Control, Part of 2010 IEEE Multi-Conference on Systems and Control. IEEE Publ., Yohohama, Japan, pp. 2380–2384.

Wu, Y., Hu, X., Hu, D., et al., 2005. Strapdown inertial navigation system algorithms based on dual quaternions. IEEE Trans. Aerosp. Electron. Syst. 41 (1), 110–132.

Yuan, J., Hou, X., Sun, C., et al., 2019. Fault-tolerant pose and inertial parameters estimation of an uncooperative spacecraft based on dual vector quaternions. Proc. Inst. Mech. Eng., Part G: J. Aerospace Eng. 233 (4), 1250–1269. https://doi.org/10.1177/0954410017751766, arXiv: https://doi.org/10.1177/0954410017751766.